Research article

Suppressing ERp57 diminishes osteoclast activity and ameliorates ovariectomy-induced bone loss via the intervention in calcium oscillation and the calmodulin/calcineurin/Nfatc1 pathway

Tao Yuan [a,1], Yi Wang [b,c,1], Haojue Wang [a], Qizhen Lu [b], Xin Zhang [b], Ziqing Li [b,c,**], Shui Sun [a,b,c,*]

[a] Department of Joint Surgery, Shandong Provincial Hospital, Cheeloo College of Medicine, Shandong University, Jinan, Shandong 250012, China
[b] Department of Joint Surgery, Shandong Provincial Hospital Affiliated to Shandong First Medical University, Jinan, Shandong 250021, China
[c] Orthopaedic Research Laboratory, Medical Science and Technology Innovation Center, Shandong First Medical University & Shandong Academy of Medical Sciences, Jinan, Shandong 250117, China

ABSTRACT

Background: Increased osteoclast activity constitutes the primary etiology of excessive bone erosion in postmenopausal osteoporosis. ERp57, otherwise referred to as protein disulfide isomerase A3 (PDIA3), plays a crucial role in the regulation of intracellular calcium signaling. This is documented to exert a profound impact on osteoclast differentiation and functionality.

Methods: To ascertain the potential role of ERp57 in disease progression, prevention, and treatment, network pharmacology and bioinformatics analyses were conducted in relation to postmenopausal osteoporosis and ERp57 inhibitor (Loc14). Then, subsequent experimental verifications were employed in vitro on osteoclast and osteoblast, and in vivo on ovariectomy (OVX) mice models.

Results: Multiple enrichment analyses suggested that the "calcium signaling pathway" may constitute a potential avenue for therapeutic intervention by Loc14 in the treatment of postmenopausal osteoporosis. In vitro experiments demonstrated inhibition of ERp57 could block osteoclast differentiation and function by interfering with the expression of osteoclast marker genes (Traf6, Nfatc1, and Ctsk). Further mechanisms studies based on calcium imaging, qPCR, and WB established that ERp57 inhibitor (Loc14) could obstruct calcium oscillation in osteoclast precursor cells (OPCs) by limiting the entry sources of cytosolic Ca^{2+} and interfering with calmodulin/calcineurin/Nfatc1 pathway. Evidence from Micro-CT scanning and double calcein labeling confirmed that the application of Loc14 in vivo could alleviate bone loss and partially reversed the osteogenic impairment caused by OVX in mice.

Conclusions: Our findings proved the suppressive effects of Loc14 on osteoclastogenesis via attenuating calcium oscillation and associated singling pathways, providing ERp57 as a potential therapeutic target for postmenopausal osteoporosis.

  * Corresponding author.
 ** Corresponding author.
    E-mail addresses: liziqing@sdfmu.edu.cn (Z. Li), sunshui@sdfmu.edu.cn (S. Sun).
  [1] Tao Yuan and Yi Wang contributed equally to this work.

1. Introduction

Osteoporosis is a systemic metabolic skeletal disease, featured by loss of bone mass, disruption of bone microarchitecture and increased propensity of fragility fracture [1,2]. Investigations undertaken by the Chinese Center for Disease Control and Prevention (CDC) reveal that about 5 % of men aged 40 years or older are affected by osteoporosis in mainland China, while the incidence rate rises to 20.6 % in women [3]. Among elderly women, postmenopausal osteoporosis is the most common type, and one in three women worldwide over the age of 50 might experience an osteoporotic fracture in their lifetime [4]. Although the exact pathological process behind osteoporosis is yet to be fully understood, excessive bone erosion due to overactivation of osteoclasts is largely considered to contribute to the disease progression [5,6].

Osteoclast, originating from the hematopoietic stem cell, plays a crucial role in bone resorption [7–9]. This resorptive activity of osteoclast allows for a bone matrix that not only fulfills its structural duties but also contributes to calcium homeostasis per requirements. A variety of signaling pathways are involved in the regulatory process, among which, calcium (Ca^{2+}) signaling is pivotal for both Ca^{2+} homeostasis and osteoclast biology [10]. Substantial evidence indicates that Ca^{2+} oscillation, a term referring to the fluctuation in cytosolic Ca^{2+} concentration and the trigger for Ca^{2+} signaling [10,11], plays an indispensable role in osteoclast differentiation and function [12–14]. The regulation of Ca^{2+} oscillation is a complex process implicating multiple channels and pathway. An increase in cytosolic Ca^{2+} triggers its binding to calmodulin (Calm), initiating the activation of target proteins including calcineurin and Ca^{2+}/calmodulin-dependent protein kinases II (CaMKII). This activation ultimately results in the translocation of Nfatc1 into the nucleus and subsequently initiates osteoclast differentiation [15,16]. Since pathological conditions of bone loss are more prevalent due to excessive osteoclast activity, several studies have been gathered suggesting that interfering with calcium oscillation could regulate osteoclast differentiation and functionality [17,18]. Thus, targeting the core regulator of Ca^{2+} signaling pathway might present an effective way to prevent or treat osteoporosis.

Protein disulfide-isomerase A3 (PDIA3), also known by different names including ERp57, $1\alpha,25(OH)_2D_3$-membrane-associated rapid response to steroid (MAARS), or GRP58, is a ubiquitous endoplasmic reticulum (ER) thiol-dependent oxidoreductase [19,20]. As a pleiotropic member of the PDIs family, ERp57 not only functions as an isomerase enabling the proper folding of glycoproteins, but also plays a vital role in the regulation of cellular Ca^{2+} homeostasis [20]. Notably, ERp57 is located in several cellular compartments, most dominantly in the ER, but also in the cell membrane and mitochondria [20]. Within the ER, ERp57 modulates store-operated calcium entry (SOCE) by interacting with Calreticulin (Calr) and stromal interaction molecule 1 (Stim1). Upon depletion of ER Ca^{2+} store, the complex of Stim1-Calr-ERp57 within the ER dissociates, leading to the aggregation of Stim1. This, in turn, translocates to ER-plasma membrane junction. Subsequently, Stim1 binds to calcium release-activated calcium modulator 1 (Orai1) and transient receptor potential canonical 1 (TRPC1) which are located on the cell membrane, and triggers an influx of extracellular Ca^{2+}, aiding the refilling of ER Ca^{2+} storage. This entire process modulates a plethora of biological process, many of which are closely related to musculoskeletal tissues [20,21].

Over the last decades, owing to the soaring advancements in bioinformatics databases, the utilization of multiple public platforms has greatly expedited the identification of target genes and the development of novel drugs [22]. Employing bioinformatics methodologies such as molecular docking, Gene Ontology (GO), Kyoto Encyclopedia of Genes Genomes (KEGG) enrichment analysis, and protein-protein interaction (PPI) network, has provided theoretical guidance for biological research based on predictions of the relationship between genes, drugs, and diseases.

In current study, we utilized publicly available bioinformatics databases to establish a close relationship between the ERp57 inhibitor-Loc14 and osteoporosis. We then corroborated in vitro that ERp57 inhibitor had a negative impact on osteoclast differentiation via the suppression of calcium oscillation. Subsequently, the in vitro effects were further validated in the ovariectomy (OVX) -induced postmenopausal osteoporosis mice model.

2. Results

2.1. ERp57 may involve in the pathogenesis of postmenopausal osteoporosis via calcium signaling

To investigate the involvement of ERp57 in the disease pathogenesis from the bone resorption aspect, we first explore the expression pattern of ERp57 during osteoclastogenesis by gathering protein samples at varying stages of osteoclast induction. WB results evidently showed an increase in ERp57 protein levels, correlating with osteoclast differentiation and maturation (Fig. 1A). Thereafter, a specific inhibitor of ERp57, known as Loc14 [23–25], was employed in the study from the view of disease intervention. Molecular docking analysis was undertaken to ascertain Loc14's prospective binding mode to ERp57 according to the pharmaceutic structure (Fig. 1B), and thereby predict the docking site (Fig. 1C). Following this, a remarkable inhibitory effect of Loc14 (5 μM) on the expression level of ERp57 in osteoclast precursor cells was confirmed via WB (Fig. 1D and E).

Moreover, bioinformatic analysis was conducted to uncover the correlation between ERp57 inhibitory targets (Loc14) and postmenopausal osteoporosis-associated causative genes. The predicted targets of Loc14 were acquired from SwissTargetPrediction databases, while causative genes relating to postmenopausal osteoporosis were identified from CTD database. A Venn diagram analysis revealed a total of 81 overlapping genes between the predicted targets of Loc14 and the postmenopausal osteoporosis-associated causative genes (Fig. 1F). In an attempt to shed light on the potential underlying mechanisms of Loc14 in the treatment of postmenopausal osteoporosis, GO and KEGG analyses were conducted based on the 81 overlapping targets, and the top 5 significant terms were exhibited (Fig. 1G–J). The overlapping targets, combined with the results from biological process (BP), cell component (CC), molecular function (MF), and KEGG analysis, were found to be involved mainly in G-protein coupled receptor (GPCR) pathways and
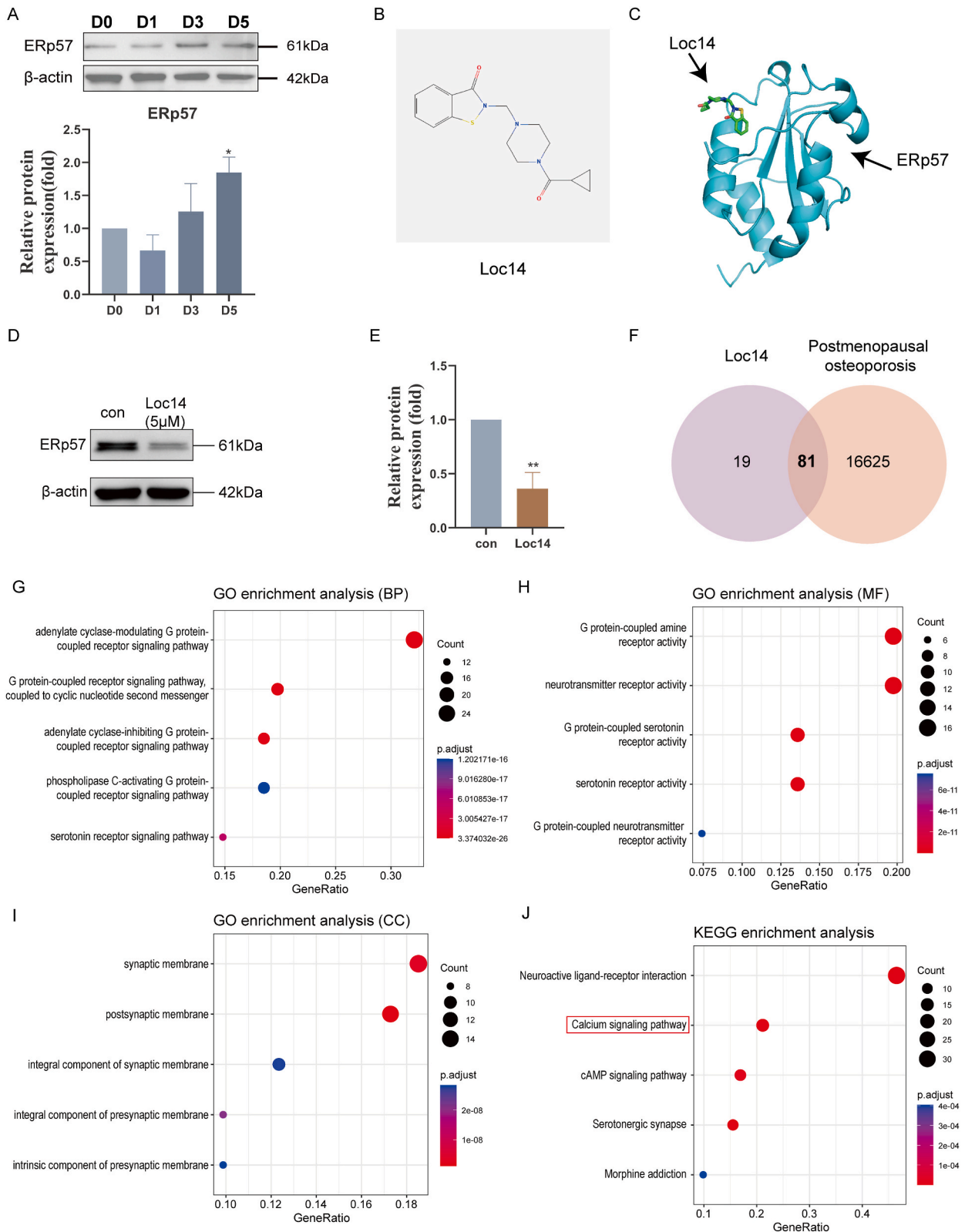
(caption on next page)

Fig. 1. ERp57 may involve in the pathogenesis of postmenopausal osteoporosis via calcium signaling. (A) Western blot (WB) assay showed increased ERp57 expression level along with osteoclast differentiation. Quantitative analysis was performed on bands and normalized to β-actin. Full-length gels are presented in Supplementary material 5: Fig. S1. (B) Molecular structure of Loc14. (C) Molecular docking of Loc14 with ERp57. (D–E) WB showed ERp57 protein levels in control and Loc14 (5 μM)-treated groups. Quantitative analysis was performed on bands and normalized to β-actin. Full-length gels are presented in Supplementary material 5: Fig. S2. (F) Venn diagram identified 81 Loc14-target genes associated with postmenopausal osteoporosis. (G–I) Gene Ontology (GO) enrichment analyses exhibited the top 5 terms of biological process (G), cell component (H), and molecular function (I), based on the 81 overlapping genes. (J) Kyoto Encyclopedia of Genes and Genomes (KEGG) analysis presented the top 5 enriched pathways. Data were presented as means ± SD (n = 3, *p < 0.05, **p < 0.01).

calcium signaling pathway (Fig. 1G–J). Considering the intimately crosstalk between GPCR and calcium signaling has long been reported [26,27], our findings collectively indicate a potential role for ERp57 in the development of postmenopausal osteoporosis, possibly via the regulation of calcium signaling during osteoclastogenesis.

2.2. Loc14 impedes RANKL-induced osteoclast differentiation and function

We next ask whether suppression of ERp57 could affect osteoclastogenesis so as to intervene the progress of postmenopausal osteoporosis. To achieve that, CCK-8 assay was performed to determine the optimal concentration of Loc14 for the subsequent experiments, and gradient concentrations (0.3125, 0.625, 1.25, 2.5, 5, 10 and 20 μM) of Loc 14 were applied to treat BMMs or OPCs. The results exhibited no discernible toxicity upon treatment of BMMs or OPCs with Loc14 at concentrations ranging from 0.3125 to 10 μM (Fig. 2A–B). We further established the impact of Loc14 on osteoclast differentiation and function. TRAP staining revealed that BMMs in the control group differentiated into large, TRAP-positive multinucleated OCs, while Loc14 treatment noticeably reduce the number of OCs with 6–9 nuclei and 10 more nuclei in a dose-dependent manner (Fig. 2C and F).

The investigation was then expanded to evaluate the effect of Loc14 on osteoclast function, wherein the F-actin ring formation and acid secretion ability of mature osteoclasts were assessed for this purpose. Phalloidin staining was performed to confirm the influence of Loc 14 on F-actin ring formation, and the results showed that while 77.6 % of the osteoclasts in the control group possessed intact F-actin ring, the percentage dropped to below 20 % in the 5 μM Loc14 group (Fig. 2D and G). The acid secretion ability of mature osteoclasts was subsequently evaluated by AO staining. As seen in Fig. 2E, higher acidification levels were observed in the control group, contrasting with the reduced ratio of red to green fluorescence intensity in Loc14-treated group (Fig. 2E and H). Collectively, these results confirm that Loc14 impedes the formation and bone absorption capability of mature osteoclasts in a dose-dependent manner. In addition, 5 μM of Loc14 has been determined as the optimal concentration for subsequent experiments.

2.3. Loc14 suppresses the expression of osteoclast marker genes and Ca^{2+} oscillations

To preliminary elucidate the mechanism of Loc14 in inhibiting osteoclast differentiation and function, both the transcriptional and translational levels of osteoclast marker genes were assessed via qPCR and WB. The qPCR assay validated that the transcriptional level of differentiation-related (*Nfatc1*, *Traf6*) and function-related (*Ctsk*) marker genes were significantly downregulated upon Loc14 intervention (Fig. 3A, B and C). Furthermore, WB results also corroborated that the protein levels of Nfatc1 and Ctsk were also reduced after Loc14 treatment (Fig. 3D, E and F). In brief, these evidences prove that Loc14 attenuates osteoclastogenesis by suppressing osteoclast marker genes at both mRNA and protein levels.

Considering the necessity of Ca^{2+} oscillation as an upstream regulator in the RANKL-induced Nfatc1 auto-amplification and osteoclast differentiation [28], and the vital role of ERp57 in maintaining cellular Ca^{2+} homeostasis [20,29], we therefore ask whether the inhibitory effect of Loc14 on the marker genes and cellular behaviors are originated from the impact on Ca^{2+} oscillation. To validate this theory, we assessed Ca^{2+} oscillation in OPCs by employing the Fluo-4 AM fluorescent probe. The results demonstrated sustained high-amplitude Ca^{2+} oscillations in the control group, whereas Ca^{2+} oscillations in the Loc14-treated group were minimally detectable (Fig. 3G and H; Supplementary videos 1 and 2). All these data suggested the impaired phenotype of osteoclast may be attributed to Loc14-caused suppression of marker genes via its impact on intracellular Ca^{2+} oscillation.

Supplementary video related to this article can be found at https://doi.org/10.1016/j.heliyon.2024.e35374

2.4. Loc14 limits the entry sources of cytosolic Ca^{2+} in OPCs

Given that Ca^{2+} oscillations originate from periodic influxes of free Ca^{2+} and continuous cycles of Ca^{2+} release and reuptake from the intracellular stores, especially ER, we therefore investigated whether the inhibitory effect of Loc14 on Ca^{2+} oscillation affected these two primary sources. To determine the effect of Loc14 on ER Ca^{2+} release, TG was applied to treat OPCs, inducing Ca^{2+} leakage from ER by inhibiting sarco/endoplasmic reticulum Ca^{2+}-ATPase (SERCA). Dramatically soared fluorescence intensity was observed in control OPCs after TG stimulation, while only a slightly elevation was noted in Loc14-treated OPCs (Fig. 4A and B, Supplementary videos 3 and 4). Additionally, fluorescence intensity decayed more rapidly in Loc14-treated OPCs post-peak than the control group (Fig. 4B). Significant differences of OPCs between the two groups were captured after 15s and 30s of TG application (Fig. 4C).

Supplementary video related to this article can be found at https://doi.org/10.1016/j.heliyon.2024.e35374

Then we evaluated the influence of Loc14 treatment on extracellular Ca^{2+} influx. When the cytosolic Ca^{2+} fluorescence intensity reached to a stable baseline in Ca^{2+} free ISO, ISO with 2.6 mM $CaCl_2$ were added to arise extracellular Ca^{2+} influx. Our results exhibited the fluorescence intensity increased speedily in control OPCs after ISO with 2.6 mM $CaCl_2$ loaded. However, a subtle decline
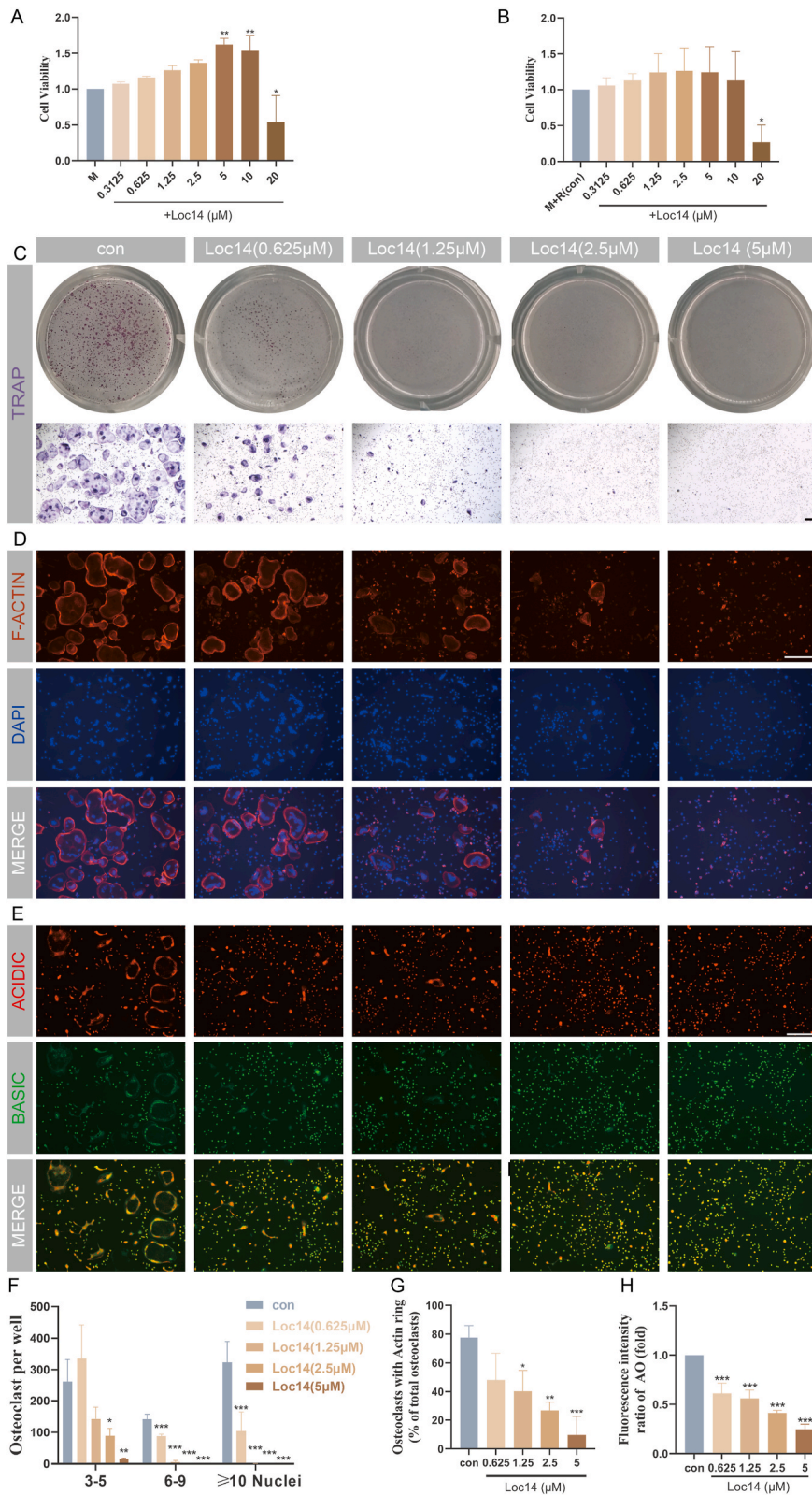
(caption on next page)

Fig. 2. Loc14 impedes RANKL-induced osteoclast differentiation and function. (A) CCK-8 assay detected the viability of bone marrow-derived macrophages (BMMs) or osteoclast precursor cells (OPCs) (B) after treated with Loc14 in gradient concentration (0–20 μM) for 24h. (C) TRAP staining of osteoclasts under Loc14 treatment with gradient concentration (0, 0.625, 1.25, 2.5 and 5 μM), and (F) the number of TRAP-positive osteoclasts with different nuclei (n = 3, 6–9, and ≥10) were counted. Scale bar = 100 μm. (D) F-actin rings for osteoclasts with or without Loc14 treatment after osteoclast induction for 5 days. The F-actin rings (red) and nuclei (blue) of control and Loc14-treated group were stained with phalloidin-iflour 594 and DAPI, and visualized by a fluorescence microscope. Scale bar = 100 μm. (G) Quantification of osteoclasts with F-actin rings per group. (E) Acridine orange (AO) staining after osteoclast induction for 5 days with Loc14 treatment. Scale bar = 100 μm. (H) The ratio of fluorescence intensity (red to green) of AO staining was quantitatively measured using Image J software. Data were shown as means $\pm$ SD (n = 3, *p < 0.05, **p < 0.01, ***p < 0.001). (For interpretation of the references to color in this figure legend, the reader is referred to the Web version of this article.)

signal followed by a relative stable fluorescence plateau was observed in Loc14-treated OPCs (Fig. 4D and E, Supplementary videos 5 and 6). Also, significant differences occurred after 5s and 150s of 2.6 mM $CaCl_2$ loaded (Fig. 4F).

Supplementary video related to this article can be found at https://doi.org/10.1016/j.heliyon.2024.e35374

Collectively, these data suggested inhibition of ERp57 represses both ER Ca^{2+} release and extracellular Ca^{2+} influx, leading to inhibition of calcium oscillation of OPCs, eventually attenuates osteoclast formation.

2.5. Loc14 restrains Ca^{2+} oscillation by affecting SOCE, Ca^{2+}/Calm/calcineruin and MAPK pathways

Several published works have reported that ERp57 is closely related to the SOCE pathway by its interaction with Calr [21]. In addition, Ca^{2+}/calmodulin-dependent kinase II (CaMKII) is required in ERp57-mediated rapid actions of 1,25-dihydroxy vitamin D_3 [20,30]. Combined with the result of the KEGG analysis (Fig. 1J), we thus hypothesized the inhibitory effect of Loc14 on Ca^{2+} oscillation may also be directly from its impact on SOCE and -related signaling pathways. The mRNA levels of related genes were quantified and results revealed that genes including SOCE-related (*Calr*, *Stim1*, *Orai1*, and *Trpc1*) and Ca^{2+}/Calm/calcineruin pathway-related (*Calm* and *Calcineurin*), were all significantly downregulated under Loc14 stimulation (Fig. 5A). Among them, the critical regulators were further corroborated by WB analysis at the protein levels which were consistent with the qPCR data (Fig. 5B–G).

Binding RANKL to RANK activates a broad range of signal cascade, including calcium signaling pathway, NF-κB and mitogen-activated kinase (MAPK) pathways [31]. And MAPK signaling pathway is reported to be activated following calcium influx in several cell types, such as neuron [32]. We therefore detect the activation of Loc14 on MAPK signaling pathway. WB showed Loc14 inhibited phosphorylation of ERK and JNK in MAPK pathway (Fig. 5H–J).

In summary, these findings reveal Loc14's capacity to constrain the SOCE and Ca^{2+}/Calm/calcineurin pathway, thereby reducing Ca^{2+} oscillation and impeding the activation of MAPK pathway, ultimately suppressing osteoclast differentiation and function.

### 2.6. Loc14 protects against bone loss in OVX mice models

Based on the results acquired from our bioinformatic analysis and in vitro experiments, we further validate the therapeutic effects of Loc14 in vivo using established OVX mouse models. Mice in the OVX + Loc14 group received an intraperitoneal injection of Loc14 (5 mg/kg) every two days, whereas the sham and OVX groups were administered a normal saline injection following the same protocol, one week postoperatively up till the fourth weeks. Following sacrifice, left femurs were collected for micro-CT analysis. Three dimensional (3D) images showed sparse trabecular bone in the OVX groups compared with the sham group. However, treatment with Loc14 appeared to prevent this bone loss (Fig. 6A). A notable reduction was observed in the BV/TV and Tb.N in the OVX group when compared to the sham group while the Tb.Sp was significantly enlarged. Treatment with Loc14, on the other hand, increased the BV/TV and Tb.N, and reduced the Tb.Sp in comparision with the OVX group. Despite this, no significant difference was noted in the Tb.Th between all three groups (Fig. 6B–E). Overall, these data highlight the therapeutic effects of Loc14 on OVX-induced osteoporosis.

2.7. Loc14 dampens TRAP positive osteoclasts formation in vivo

To further delineate the role of Loc14 in osteoclastogenesis in vivo, cryosections of left femurs from different groups were stained with TRAP solution, then counterstained with methyl green or Weigert hematoxylin solution. As showed in images, obviously increased numbers of TRAP positive osteoclasts and sparse trabecular bones were observed in distal femurs of OVX group, while OCs numbers were decreased and trabecular bones were dense under Loc14 treatment (Fig. 7A–D). To sum up, evidences from micro-CT and histological assessments indicated that Loc14 ameliorates OVX-induced osteoporosis by dampening osteoclast formation in vivo.

2.8. Loc14 has no influence on osteoblastic differentiation in vitro but enhances osteogenesis in vivo

The basic multicellular unit (BMU), which is composed of osteoclast, osteoblasts, osteocytes and bone lining cells, orchestrates the bone remodeling process [33,34]. We therefore detected the effect of Loc14 treatment on other cell types in BMU. Loc14 showed no significant cytotoxicity upon the treatment of osteoblastic precursor cells within the indicated concentration (0–20 μM) (Fig. 8 A). Drawing on the results of ALP staining (Fig. 8B) and WB of ALP protein (Fig. 8C–D), Loc14 in 5 μM has no promotion or inhibition on osteoblastic differentiation in vitro. Interestingly, double calcein labeling showed enhanced osteogenic process and higher mineral
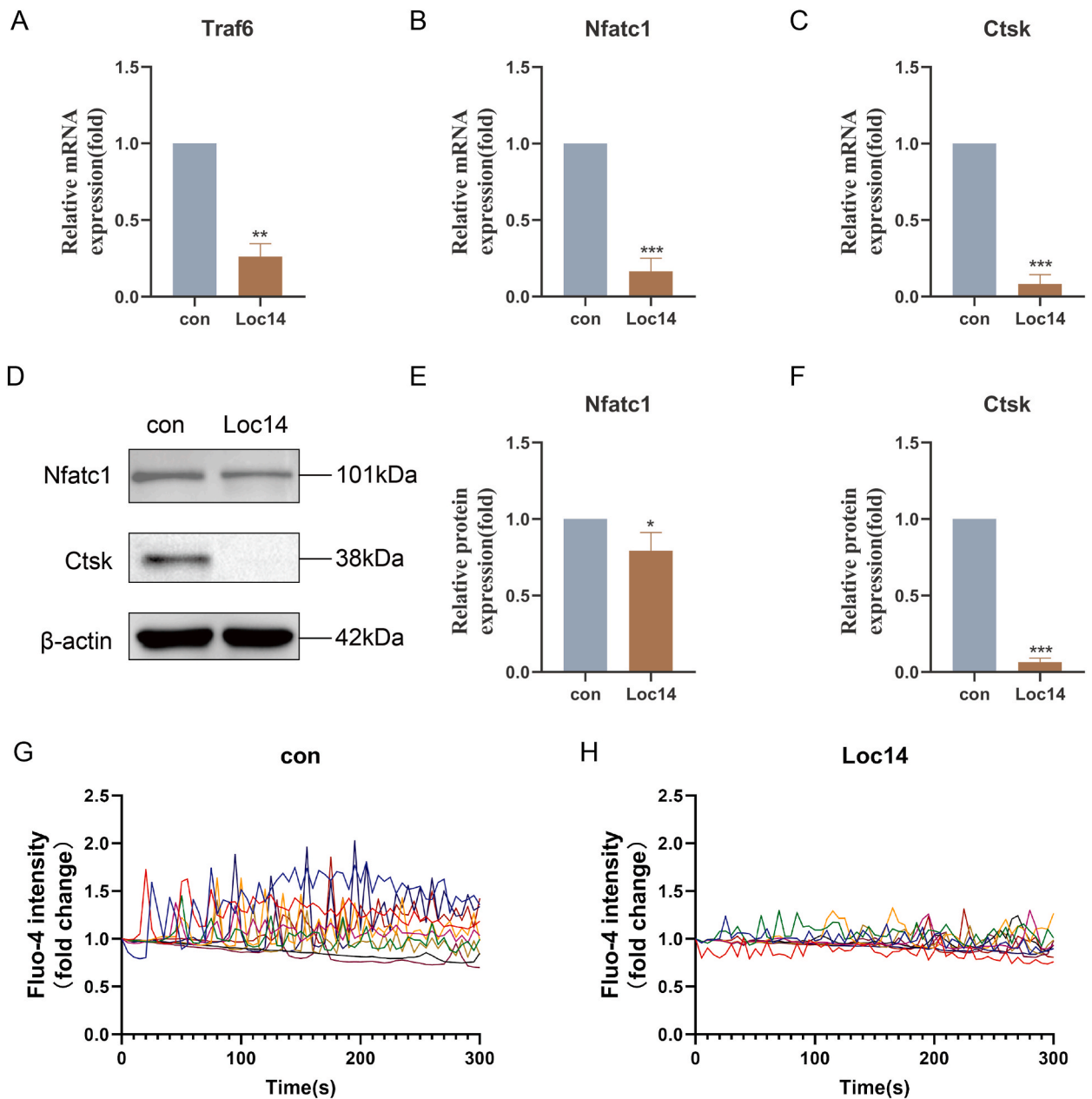
Fig. 3. Loc14 suppresses the expression of osteoclast marker genes and Ca^{2+} oscillations. (A–C) qPCR analysis of Traf6, Nfatc1 and Ctsk transcript levels in control and Loc14 (5 μM)-treated groups. Data were normalized to GAPDH and presented as mean ± SD (n = 3). (D–F) WB showed expression levels of Nfatc1 and Ctsk in control and Loc14-treated groups. Data were normalized to β-actin and presented as mean ± SD (n = 3). Full-length gels are presented in Supplementary material 5: Figure S3 (G-H) Ca^{2+} oscillations of OPCs after osteoclast induction for 24h with or without Loc14 (5 μM) treatment. Sparking cells were traced, calculated, and plotted over time using different colors (n = 10 cells in each group). (*p < 0.05, **p < 0.01, ***p < 0.001). (For interpretation of the references to color in this figure legend, the reader is referred to the Web version of this article.)

apposition rate (MAR) and bone formation rate (BFR) in OVX + Loc14 group compared to the OVX group (Fig. 8E–G). TRAP and hematoxylin staining further demonstrated that Loc14 treatment partially mitigated the reduction in femoral cortical thickness caused by OVX, and concurrently increased the number of osteoblasts (Fig. 8H).

3. Discussion

ERp57, a multifaceted protein that belongs to the PDI family, has a diverse nature with multiple localizations and functions in various physiological and pathological processes, including catalyzing the formation of intra- or intermolecular disulfide bonds during
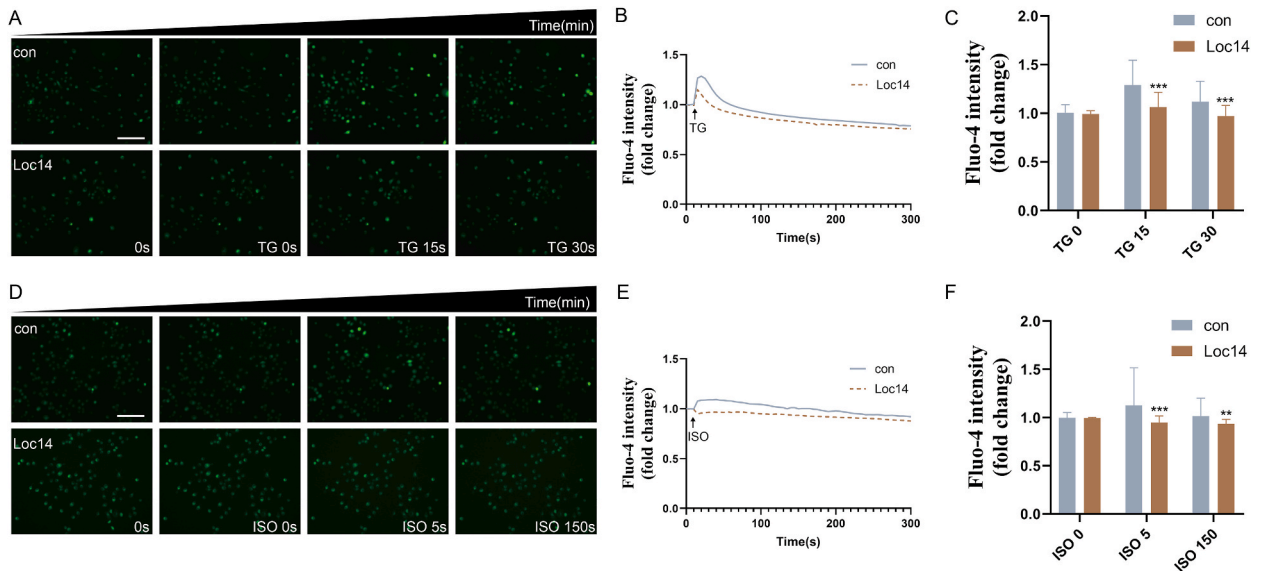
Fig. 4. Loc14 limits the entry sources of cytosolic Ca^{2+} in OPCs. (A) Representative images of intracellular Ca^{2+} fluorescence in OPCs before (0s) and after stimulation of 1 mM TG (started from TG 0s). OPCs were incubated in Ca^{2+}-free ISO to reach the baseline level of cytosolic Ca^{2+}, and then treated with TG in Ca^{2+}-free ISO to trigger Ca^{2+} leakage from ER. Scale bar = 100 μm. (B) Fluorescence intensity curves of OPCs. Arrow indicates the time point of TG application. Data is expressed as fold change of fluo-4 intensity normalizing to each cell's initial fluorescence intensity (n = 30 cells per group). (C) Quantitative analysis of fluo-4 intensity at indicated time point, under TG treatment. ***p < 0.001 versus Loc14 treated cells (n = 90 cells per group). (D) Representative images of intracellular Ca^{2+} fluorescence in OPCs before (0s) and after stimulation of ISO with 1.3 mM $CaCl_2$ (started from ISO 0s). OPCs were incubated in Ca^{2+}-free ISO to reach the baseline level of cytosolic Ca^{2+}, and then treated with ISO to evoke extracellular Ca^{2+} influx. Scale bar = 100 μm. (E) Fluorescence intensity curves of OPCs. Arrow indicates the time point of ISO application. Data is expressed as fold change of fluo-4 intensity normalizing to each cell's initial fluorescence intensity (n = 30 cells per group). (F) Quantitative analysis of fluo-4 intensity at indicated time point, under $2 \times Ca^{2+}$ ISO treatment. **p < 0.01, ***p < 0.001 versus Loc14 treated cells (n = 90 cells per group). Data were shown as mean ± SD.

glycoprotein folding [35], aiding the assembly of class I major histocompatibility complexes [36], facilitating platelet aggregation and thrombosis [37], and maintaining calcium homeostasis [20,38]. Limited studies have suggested its potential involvement in skeletal diseases. In our previous work, we observed inhibition of PDIA1(another member of PDI family) could alleviate OVX-induced bone loss through the repression of osteoclast differentiation and function by readjusting cellular redox state [5]. Given the substantial structural and functional overlap between PDIA1 and ERp57 [20], there is a need to examine the latter's role in bone resorption, which remains unclear. This study is the first to provide multiple bioinformatics evidence that the ERp57-regulated calcium signaling may be involved in the osteoclast differentiation and function, significantly impacting the pathological development of postmenopausal osteoporosis. Moreover, from a translational approach, the ERp57 inhibitor-Loc14 [23–25], was employed to assess its preventative and therapeutic efficacy. It was observed that Loc14 notably suppressed osteoclastogenesis and mitigated OVX-induced bone loss by decreasing Ca^{2+} oscillation through multiple calcium signaling pathways.

Recent studies have suggested the potential involvement of ERp57 in the skeletal development. A study by Wang et al., in which heterozygous-knockout Pdia3$^{+/-}$ mice were developed, presented evidence of impaired bone formation and osteoblast differentiation, in contrast to their wild type counterpart [39,40]. Linz et al. reported cartilage-specific ERp57 knockout mice exhibited phenotypes including enlarged growth plates, extended hypertrophic zones, delayed osteoclast recruitment, reduced proliferation, and enhanced apoptosis of chondrocytes [41]. In our study, changes in osteoclast morphology and behavior are linked to the influence of ERp57 on key genes and proteins. We demonstrated that the ERp57 inhibitor, Loc14, significantly impeded the transcription of osteoclast differentiation-related (*Traf6, Nfatc1*) and function-related (*Ctsk*) marker genes. Further WB assessments on the protein expression of Nfatc1 and Ctsk were in line with the trend of qPCR data. As such, we confirmed that Loc14 diminished the differentiation and function of osteoclasts by deterring the expression of osteoclastic markers both at transcription and translation levels, subsequently providing protective effects against bone loss in OVX mice models.

We identified that Ca^{2+} oscillation is a critical contributor to the regulatory role of ERp57 in osteoclastogenesis. Ca^{2+} oscillation pertains to the dynamic fluctuations of Ca^{2+} level within the cytoplasm, governed by multiple channels and transporters [10,42]. Intensifying Ca^{2+} oscillation is a core process that mediates osteoclast differentiation and bone resorption [10,43]. Ca^{2+} oscillation is primarily triggered by two routines: 1) Ca^{2+} release from the intracellular Ca^{2+} store such as ER, 2) an influx of extracellular Ca^{2+}. SOCE is an essential mechanism between the two routines for the refilling of ER Ca^{2+} store [44], relying on Ca^{2+} release-activated Ca^{2+} channels (CRAC) composed of various ion channels including Stim1, Orai1, and Trpc1 [10,45]. Among these channels, Stim1 is crucial to elicit SOCE [45,46]. Several published works suggested ERp57 is deeply involved in SOCE regulation via its interaction with Stim1 [21,47]. Upon ER Ca^{2+} store is depleted due to Itpr1 induced Ca^{2+} release, ERp57 dissociates with Stim1, enabling Stim1 to dimerize
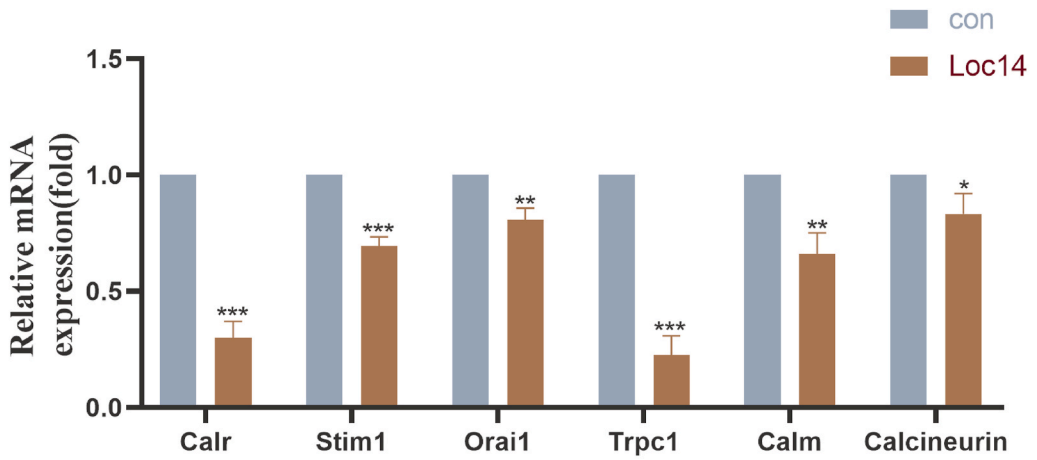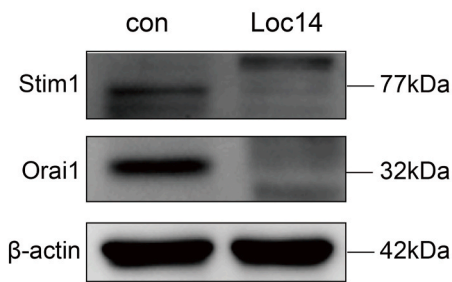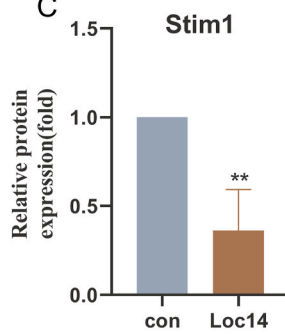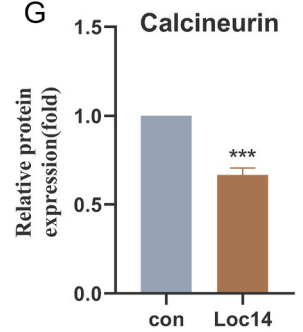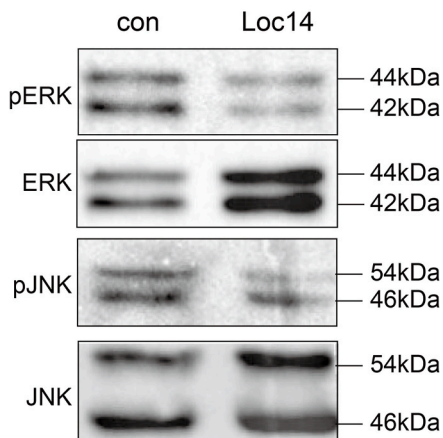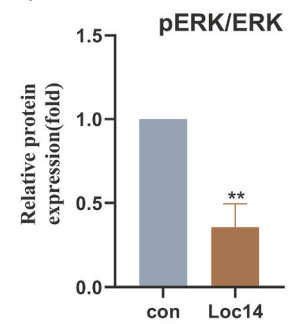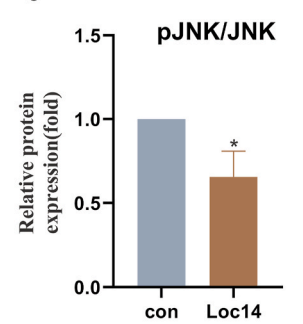
(caption on next page)
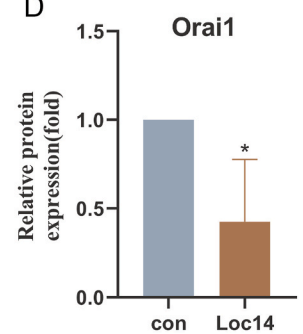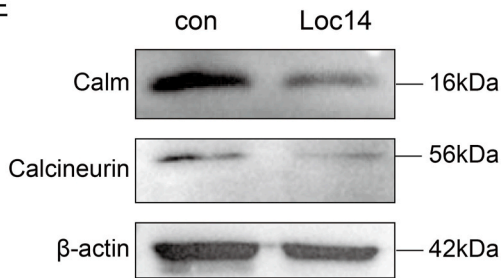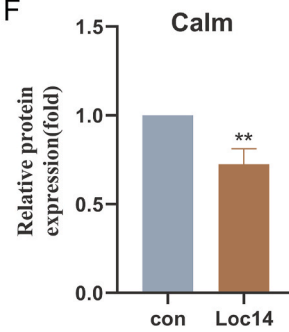
Fig. 5. Loc14 restrains Ca^{2+} oscillation by affecting SOCE, Ca2+/Calm/calcineruin and MAPK pathways. (A) qPCR analysis of Calr, Stim1, Orai1, Trpc1, Calm, and Calcineurin transcript levels in control and Loc14 (5 μM)-treated groups. Data were normalized to GAPDH and presented as mean ± SD (n = 3). (B–G) WB showed expression levels of Stim1, Orai1, Calm and Calcineurin in control and Loc14 (5 μM)-treated groups. Full-length gels are presented in Supplementary material 5: Figs. S4 and S5. (H–J) WB showed expression levels of pERK, ERK, pJNK and JNK in control and Loc14 (5 μM)-treated groups. Data were normalized to β-actin and 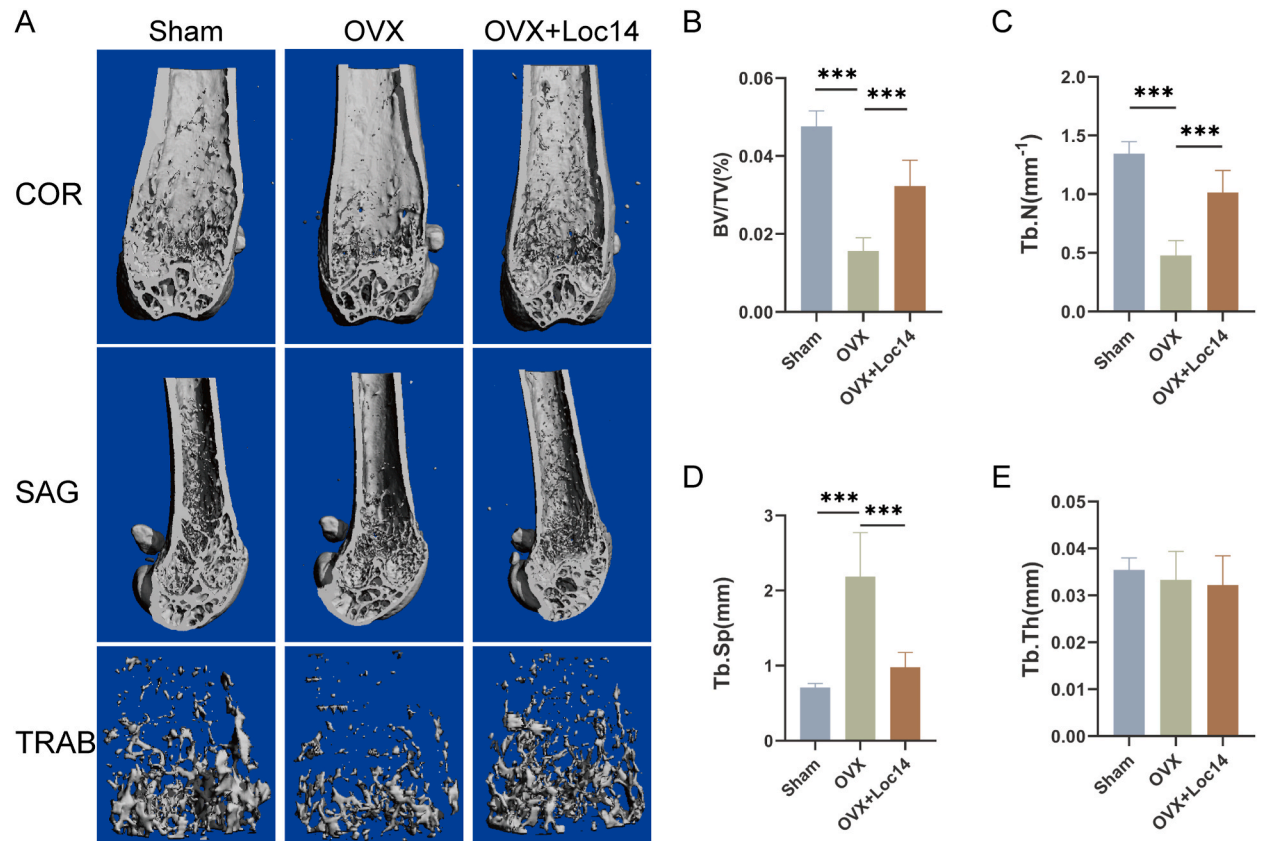presented as mean ± SD (n = 3). Full-length gels are presented in Supplementary material 5: Fig. S6. (*p < 0.05, **p < 0.01, ***p < 0.001).


Fig. 6. Loc14 protects against bone loss in OVX mice models. (A) Representative images of micro-CT of distal femurs from Sham, OVX and OVX + Loc14 (5 mg/kg) groups. (B–E) Quantitative analysis of femoral trabecular bone microstructure-related parameters, including bone volume fraction (BV/TV) (B), trabecular number (Tb.N) (C), trabecular thickness (Tb.Th) (D), and trabecular separation (Tb.Sp) (E) Data were presented as mean ± SD (n = 5 per group, *p < 0.05, **p < 0.01, ***p < 0.001).

and translocate near the plasma membrane (PM), leading to the recruitment of Orai1 hexamers into spatially confined puncta and Trpc1's insertion into the PM, and eventually evoking SOCE [21]. Interestingly, Prins et al. found ERp57-deficient mouse embryonic fibroblasts had lower TG-releasable ER Ca^{2+} stores than the normal wild-type cells [29]. Our results highlighted that the inhibition of ERp57 caused a decline in the expression of Stim1, Orai1, and Trpc1. This subsequently led to the disturbance in the efficient and timely replenishment of ER Ca^{2+} store, and moderation of TG-induced Ca^{2+} oscillation (Fig. 9).

In addition, a variety of Ca^{2+}-permeable channels within the plasma membrane manage the extracellular Ca^{2+} influx process, including voltage-operated channels (VOCs), second messenger-operated channels (SMOCs), and receptor-operated channels (ROCs) [48,49]. Among various VOCs (P/Q-type, N-type, and L-type) [50], the L-type VOCs (LTCCs) are known as key regulator of intracellular Ca^{2+} homeostasis in numerous cells, especially in osteoblasts [26,51]. Numerous studies have illustrated strong correlation between ERp57 and LTCC [52,53]. Yang et al. found ERp57 led to 1,25(OH)$_2$D$_3$-induced extracellular Ca^{2+} influx via LTCC in human aortic smooth muscle cells, and interfering with its expression weakened cellular Ca^{2+} influx through LTCC [54]. Our result is consistent with their findings. We observed that extracellular Ca^{2+} influx was attenuated upon the inhibition of ERp57. However, whether ERp57 inhibition affects the expression of LTCC subunits and other crucial proteins involved in this biological process was not investigated in this study, necessitating further analysis.

Calcineurin is another vital protein involved in converting Ca^{2+} oscillation signals to facilitate osteoclast differentiation [10]. The elevated cytosolic Ca^{2+} binds to calmodulin, resulting in the activation of calcineurin, which in turn, dephosphorylates serine residues in Nfatc1. This fuels the nuclear translocation of Nfatc1 and consequently promotes the transcription of osteoclast marker genes [43].
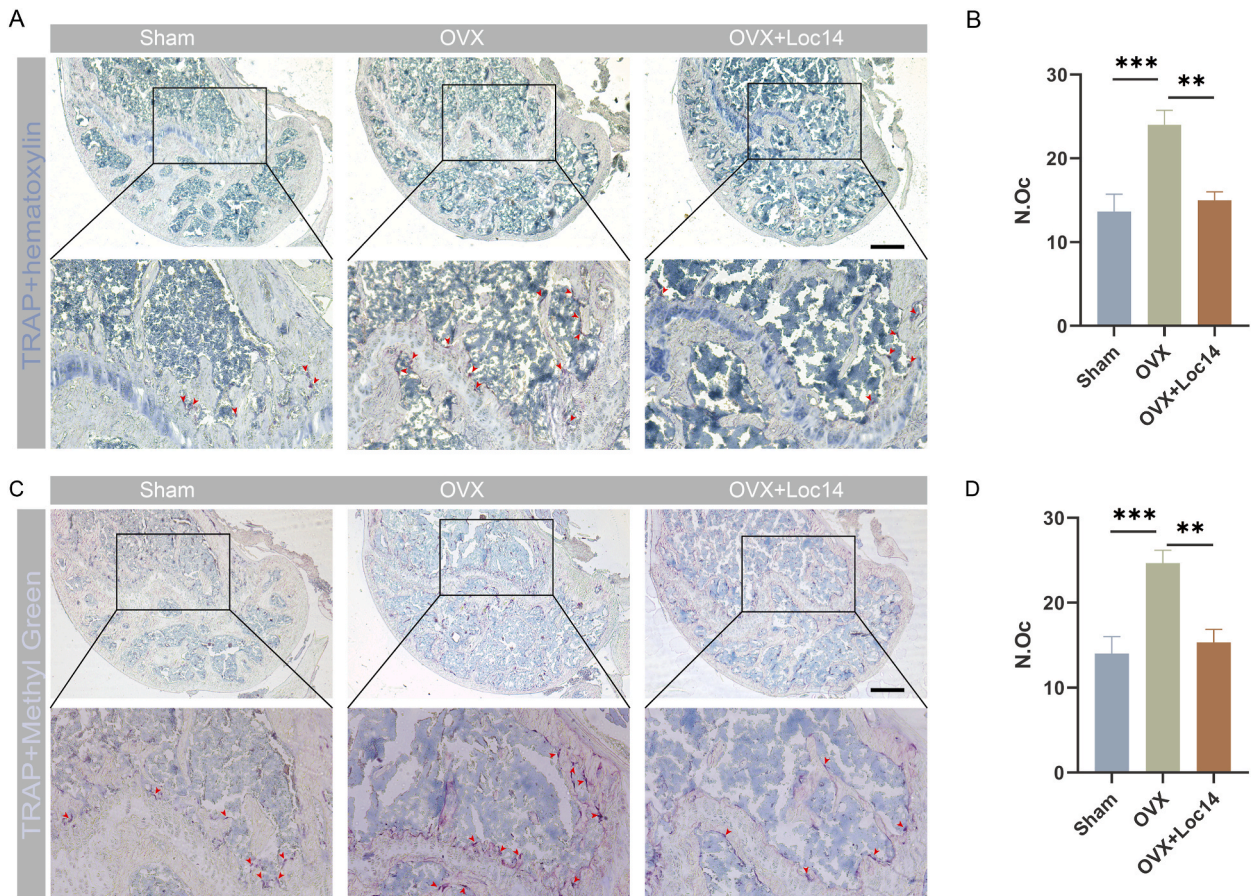
Fig. 7. Loc14 dampens TRAP positive osteoclasts formation in vivo. (A) Cryosections of femurs stained for TRAP and counterstained with Weigert hematoxylin solution. (B) Quantitative analysis of TRAP positive osteoclasts in distal femur cryosections. (C) Cryosections of femurs stained for TRAP and counterstained with methyl green. (D) Quantitative analysis of TRAP positive osteoclasts in distal femur cryosections. Red arrow heads indicate TRAP positive osteoclasts. Scale bar = 100 μm. Data were shown as mean ± SD (n = 3 per group, **p < 0.01, ***p < 0.001). (For interpretation of the references to color in this figure legend, the reader is referred to the Web version of this article.)

Yuan et al. reported that major vault protein (MVP) knockout mice exhibited a bone loss phenotype by bolstering the calcineurin-Nfatc1 signaling pathway and enhancing osteoclastogenesis, while MVP overexpression reversed pathologic bone loss in OVX mice model [6]. Likewise, Lee et al. unveiled Sphingosylphosphorylcholine suppressed RANKL-induced calcineurin activation and Nfatc1 activity, subsequently limiting Ca^{2+}/calmodulin-mediated osteoclast differentiation [55]. In our study, we grasped that the inhibition of ERp57 by Loc14 could downregulate the expression level of calmodulin and calcineurin, which further halted the nuclear translocation of Nfact1 and compromised osteoclast differentiation.

The basic multicellular unit (BMU), comprising osteoclast, osteoblasts, osteocytes and bone lining cells, orchestrates the bone remodeling process [33,34]. Although there is no reported research about ERp57's association with the BMU, the limited literature implies the crucial role of ERp57 in these cells. Since $1\alpha,25(OH)_2D_3$ directly regulates mineralization performed by osteoblasts [56], inhibiting its receptor-ERp57 is might impair osteoblast's capabilities of mineralization and differentiation, thereby affecting the formation of osteoblasts and bone lining cells. Paradoxically, several published studies have yielded contradict conclusions. For instance, Jiaxuan Chen et al. found that Pdia3-silenced MC3T3-E1 cells produced higher numbers of von Kossa-positive nodules and alizarin red-positive nodules than the WT normally functioning cells [56]. Yun Wang et al. developed Pdia3 heterozygous global knockout (Pdia3$^{+/-}$) mice and revealed that the Pdia3$^{+/-}$ mice possessed increased metaphyseal bone volume and trabeculae compared to Pdia3$^{+/+}$ mice [39]. Interestingly, a few studies have uncovered ERp57 is secreted at the site of vascular injury, promoting platelet accumulation and thrombus formation [57]. However, the exact role of ERp57 in bone remodeling process under various conditions is yet to be experimentally elucidated via at least cell-specific conditional knockout models.

In our study, the influence of 5 μM Loc14 on osteoblasts in vitro appears insignificant in comparison to normal osteoblasts. Interestingly, Loc14 appears to promote mineralization and osteogenesis under OVX condition in vivo. We believed the following reasons may be accountable for this phenomenon. Firstly, the lack of an in vitro model for postmenopausal osteoporosis limits studies to using only normal osteoblasts as a control, thereby restricting the opportunity to study the effects of Loc14 on osteoblasts under estrogen-deficient condition. Secondly, ensuring an accurate dosage of Loc14 received by osteoblasts in vivo can be challenging.
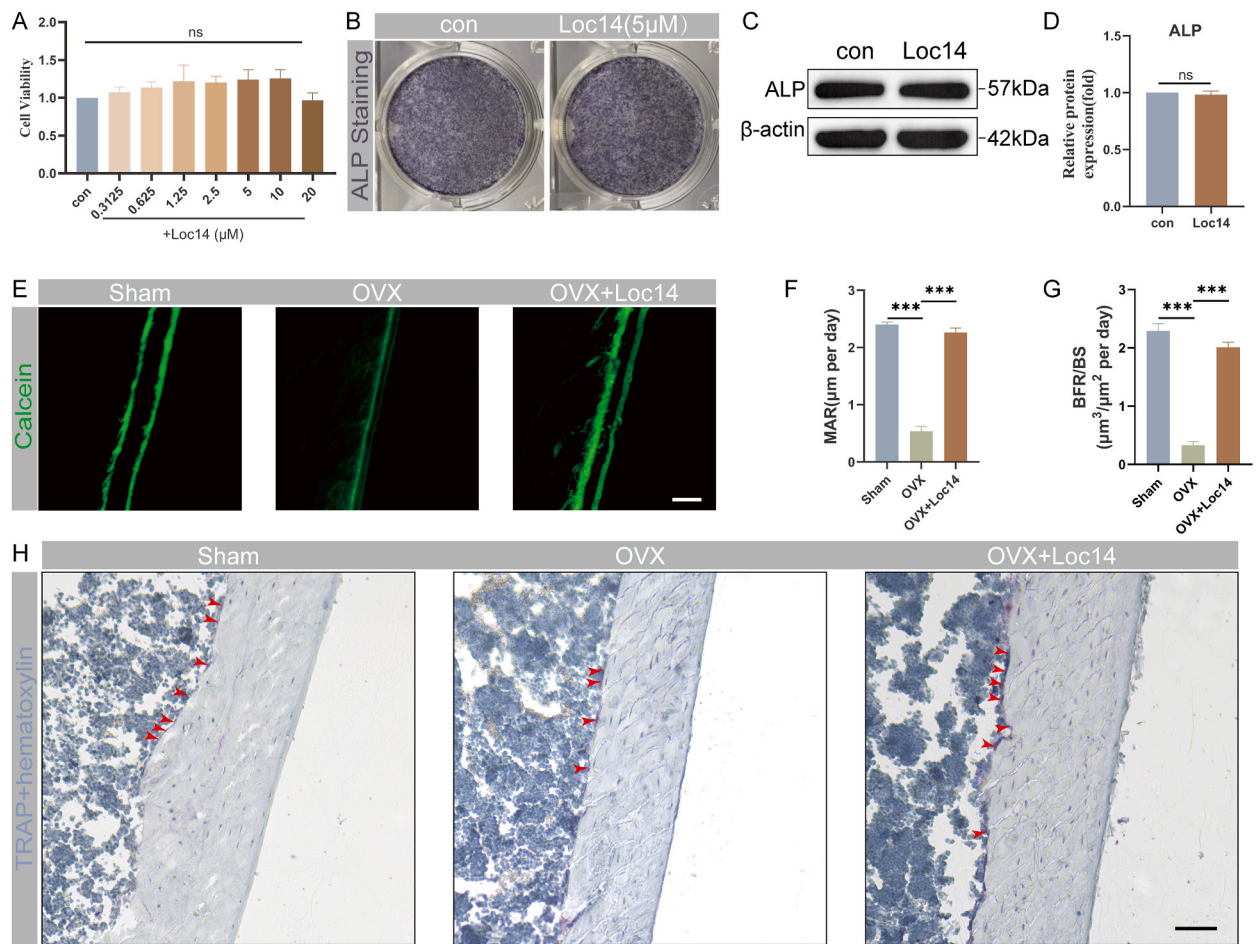
Fig. 8. Loc14 has no influence on osteoblastic differentiation in vitro but enhances osteogenesis in vivo. (A) CCK-8 assay detected the viability of osteoblastic precursor cells after treated with Loc14 in gradient concentration (0–20 μM) for 24h. (B) Representative images of ALP staining in control and Loc14 (5 μM)-treated osteoblasts. (C–D) WB analysis of ALP in control and Loc14 (5 μM)-treated osteoblasts at day 7 of osteogenic induction. Full-length gels are presented in Supplementary material 5: Figure S7 (E-G) Representative images and quantitative analysis of double calcein labeled femurs. MAR: Mineral apposition rate, BFR: Bone formation rate. Scale bar = 20 μm. (H) Representative images of femurs stained for TRAP and counterstained with Weigert hematoxylin solution. Red arrow heads indicate osteoblasts. Scale bar = 20 μm. Data were presented as mean ± SD (n = 3 per group, ***p < 0.001). (For interpretation of the references to color in this figure legend, the reader is referred to the Web version of this article.)

Lastly, bone remodeling in vivo is governed by a complicated network of multiple cells and factors—a complexity that is hard to replicate in vitro. Collectively, although Loc14 does not influence osteogenic differentiation in vitro, its facilitation of bone formation in vivo demonstrates the potential therapeutic value for postmenstrual osteoporosis.

Given the multifaceted physiological functions attributed to ERp57, the systemic administration of Loc14 may potentially interfere with these functions and induce concomitant complications. For instance, Wei Hu et al. reported that Vitamin D3 activates the auto-lysosomal degradation function by stimulating ERp57, thereby efficiently eliminating H. pylori infection in gastric epithelial cells [58]. Hence, the administration of Loc14 could compromise the anti-H. pylori effects of vitamin D3. Moreover, inhibiting ERp57 may disrupt myoblast differentiation and impair myogenesis during muscle injury [59]. Despite documented complications related to ERp57 inhibition, the exact adverse effects of Loc14 warrant additional experimental scrutiny.

The swift progression of gene-editing technology has enhanced the power and precision of tools such as the Cre/loxP technique, which helps with the investigation of cell-type-specific gene functions [60]. Developing osteoclast and osteoblast ERp57 knockdown or conditional knockout models to explore the therapeutic potential of ERp57 against postmenopausal osteoporosis is vital for a further comprehensive study, and will be the central in our future studies.

In summary, our study revealed the significant role of ERp57 in osteoclastogenesis. Additionally, ERp57 inhibitor-Loc14 could mitigate osteoclast differentiation and bone resorption, which is primarily achieved through the inhibition of Ca^{2+} oscillation by braking the SOCE and Calm-calcineurin-Nfatc1 signaling pathway. Loc14 also protected against bone loss in the OVX mouse model, thereby underscoring ERp57 as a promising therapeutic target for postmenopausal osteoporosis.
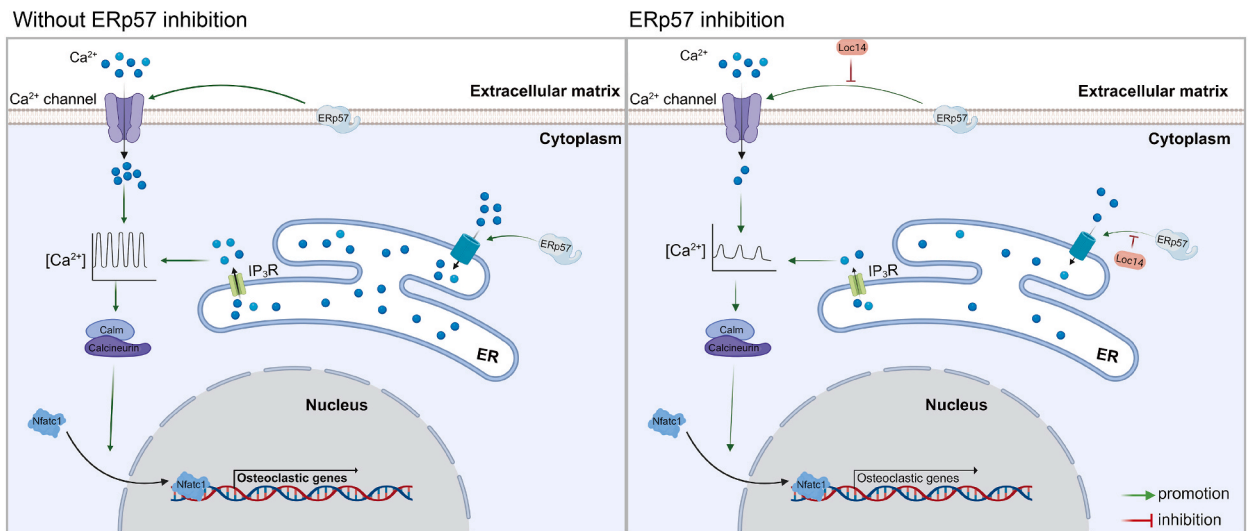
Fig. 9. Proposed mechanism of Loc14 in suppressing osteoclastogenesis via halting calcium oscillation in osteoclast precursor cells (OPCs). ER: endoplasmic reticulum; SERCA: sarco/endoplasmic reticulum Ca^{2+}-ATPase; IP_3R: inositol triphosphate (IP3) receptor; Calm: calmodulin; Nfatc1: nuclear factor of activated T cells 1; Ctsk: cathepsin K; Trap: tartrate-resistant acid phosphatase.

4. Methods

4.1. Reagents and materials

Cell culture reagents, including minimum essential medium α (α-MEM, C12571500BT, Gibco), fetal bovine serum (FBS, 10099-141C, Gibco), and penicillin/streptomycin (P/S, 15140122, Gibco), were obtained from Gibco (USA). Reagents for osteoclasts induction and stimulation included macrophage colony-stimulating factor (M-CSF, 576406, BioLegend), receptor activator of nuclear factor-κB (RANK) ligand (RANKL, 769406, BioLegend), Loc14 (V22865, Invivochem). Reagents for osteoblast induction included collagenase type II (17101-015, Gibco), 0.25 % trypsin (15050065, Gibco), dexamethasone (D4902, Sigma), β-Glycerophosphate (G9422, Sigma), and ascorbic acid (A8960, Sigma). Primary antibody used in the experiment included ERp57 (2881S, Cell Signaling Technology), Nfatc1 (A1539, Abclonal), Ctsk (sc-488353, Santa), Calcineurin (sc-17808, Santa), Calm (ab45689, Abcam), pERK (4370S, Cell Signaling Technology), ERK (4695S, Cell Signaling Technology), pJNK (ab124956, Abcam), JNK (ab179461, Abcam), ALP (DF6225, Affinity), and β-actin (sc-47778, Santa).

4.2. Molecular docking

Molecular docking was performed to predict the possible bind modes of ERp57 and Loc14. The 2D structure of Loc14 was obtained from PubChem database (https://pubchem.ncbi.nlm.nih.gov/), while the X-ray diffraction of ERp57 protein crystal structure was downloaded from the Protein Data Bank (https://www.rcsb.org/). After removing water molecules, separating ligand, and adding hydrogen by AutoDock Tools 1.5.7, the pdbqt format files of ERp57 receptor was acquired. The drug's docking region was set with default parameters by the Grid Box command, and the molecular dockings for predicting the binding mode was then performed by Vina software 1.1.2, following the visualization via PyMOL software 2.5.4.

4.3. Bioinformatics and network pharmacology analysis

The potential target genes of Loc14 were collected from SwissTargetPrediction (http://www.swisstarget prediction.ch/) databases (Supplementary material 1). Postmenopausal osteoporosis-related genes were retrieved from Comparative Toxicogenomics Database (CTD, https://ctdbase.org/) by using the term "postmenopausal osteoporosis" (Supplementary material 2). Overlapping genes of Loc14 and postmenopausal osteoporosis were identified via Venn diagrams (https://jvenn.toulouse.inra.fr/) (Supplementary material 3). Subsequently, the GO and KEGG analyses based on the overlapping genes were performed using Hiplot (https://hiplot.com.cn/) with default parameters, and the species set as "homo sapiens".

4.4. Cell culture, differentiation, and treatment

C57BL/6J mice were purchased from SiPeiFu (Beijing) Biotechnology Co., Ltd. Following the protocol approved by the Animal Care and Use Committee of Shandong Provincial Hospital Affiliated to Shandong First Medical University (Shandong, China; No.2023-034), the osteoclast culture and differentiation were conducted as our previous described [5,61]. Briefly, bone marrow cells were freshly

obtained from the femurs and tibias of C57BL/6J mice, and cultured in complete medium (α-MEM with 10 % FBS and 1 % P/S) for 16–24 h under humidified atmosphere with 5 % CO_2 in 37 °C. The non-adherent bone marrow-derived macrophages (BMMs) were then harvested and incubated in complete medium with 10 ng/ml M-CSF at a density of 2×10^5 cells/ml for 48–72 h, and changed into osteoclast-induction medium containing 10 ng/ml M-CSF and 30 ng/ml RANKL for the remaining period. Osteoclast precursor cells (OPCs) were generated after 1–3 days induction, and mature osteoclasts were obtained after 4–6 days induction. For ERp57 inhibitor treatment, Loc14 in gradient concentrations (0.3125, 0.625, 1.25, 2.5 and 5 μM) were added to each indicated group during the osteoclastogenesis process.

Primary osteoblasts were collected from mice calvaria of mice at postnatal day 4–5, as our previously performed [26]. Briefly, the isolated calvaria were cut into pieces, and then digested in digestion solution (containing 0.5 mg/ml collagenase type II and 0.05 % trypsin in α-MEM). Then cells from this digestion were cultured in complete medium in an incubator under 5 % CO_2 at 37 °C until the confluency reaching 80 %. Then adherent cells were trypsinized and reseeded for further experiments. For osteogenic differentiation, osteoblast precursor cells were treated with osteogenic medium which composed of 10^{-7} M dexamethasone, 10 mM β-Glycerophosphate, and 50 μg/ml ascorbic acid stock in complete medium.

4.5. Cytotoxicity assay

The cytotoxic effects of Loc14 on OPCs or osteoblast precursor cells were measured using the Cell Counting Kit-8 (CCK-8, E-CK-A362, Elabscience) assay [5]. Briefly, BMMs or osteoblast precursor cells were seeded in 96 well plates, and cultured in osteoclast-induction medium containing M-CSF and/or RANKL, or osteogenic medium with gradient concentrations of Loc14 (0, 0.3125, 0.625, 1.25, 2.5 and 5 μM). After 24h induction, 10 μl CCK-8 solution was added in each well, and then incubated for 2h at 37 °C and protect from light. Cell viability was measured under a microplate reader (TECAN SPARK) at the wavelength of 450 nm.

4.6. Tartrate-resistant alkaline phosphatase (TRAP) staining

TRAP staining was carried out as our previously described [5]. After 5 days osteoclast induction, cells in 24-well plates were fixed with 4 % paraformaldehyde (PFA) for 15min at room temperature, followed by twice PBS washes and stained using the Acid Phosphatase, Leukocyte (TRAP) Kit (387A, Sigma-Aldrich), as per the manufacturer's protocols. In brief, 0.5 ml Fast Garnet GBC Base Solution was mixed with 0.5 ml Sodium Nitrite Solution by gentle inversion for 30 s to produce GBC diazonium dye solution. This was followed by the preparation of solution A, which consisted of 45 ml deionized water (pre-warmed to 37 °C), 1 ml GBC diazonium dye solution, 0.5 ml Naphthol AS-Bl Phosphate solution, and 2 ml Acetate solution. The fixed cells were then incubated with solution A for 30min at 37 °C protected from light, followed by a further 30min counterstain with solution B, which was prepared by introducing 1 ml of Tartrate solution to solution A. After two washes with PBS, TRAP-positive cells were imaged by a light microscope (nib620 fl, Nexcope), and cells containing three or more nuclei were defined as mature osteoclasts.

4.7. F-actin staining

The F-actin staining was conducted in accordance with our previous publication [5]. Mature osteoclasts, cultured in 24-well plates, were fixed with 4 % PFA for 15min and then incubated with phalloidin-iflour 594 (ab176757, Abcam) at 37 °C for 2h, followed by DAPI staining of the nuclei for 5min at room temperature. After PBS wash, F-actin rings were photographed using a fluorescence microscope (EVOS M7000, Invitrogen), and quantified by calculating the ratio of mature osteoclasts possessing F-actin rings.

4.8. Acidification assay

The acidification assay was performed following our previously described protocol with minor modifications [5,62]. After 5 days osteoclast induction, cells cultured in 24-well plates were incubated in α-MEM containing a 10 μg/ml solution of acridine orange (AO, A6014, Sigma-Aldrich) for 15min at 37 °C. After three washes using α-MEM, cells in each well were imaged by a fluorescence microscope (EVOS M7000, Invitrogen) on the GFP channel (Ex/Em = 470/525 nm) and RFP channel (Ex/Em = 531/593 nm). Quantification was performed using Image J software (version 1.53q).

4.9. Alkaline phosphatase (ALP) staining

ALP staining was performed using BCIP/NBT alkaline phosphatase color development kit (C3206, Beyotime). After a 7-day osteogenic induction, osteoblasts in 24-well plates were washed gently with PBS, then stained with BCIP/NBT staining solution (containing 0.33 % BCIP solution and 0.66 % NBT solution in staining buffer) for 30min in dark.

4.10. Reverse transcription and quantitative real-time polymerase chain reaction (qPCR)

Total RNA was extracted using RNAiso Plus (9109, Takara), and then reverse transcribed into complementary DNA (cDNA) by using *EVO M-MLV* RT Premix (AG11706, Accurate Biology) kit. qPCR was conducted in a LightCycler 480II (Roche) using SYBR Green qPCR Master Mix (AG11701, Accurate Biology) following the manufacturer's cycling conditions (Denaturation: 1 cycle at 95 °C for 30 s. Amplification: 40 cycles at 95 °C for 5 s and 60 °C for 30 s. Melting: 1 cycle at 95 °C for 5 s, 60 °C for 1min and then heating to 95 °C

with 5 acquisitions per °C in a continuous mode. Cooling: 1 cycle at 50 °C for 30 s) The $2^{-\Delta\Delta CT}$ method was used to analyze the expression levels of each gene. The primer information used in the study was listed in Table 1.

4.11. Western blotting (WB)

Total cellular proteins were obtained by ice-cold radioimmunoprecipitation assay (RIPA) buffer (R0020, Solarbio) containing 1 % phosphatase (CW2383, Cwbio) and protease inhibitors (CW2200, Cwbio). Protein concentrations were determined by BCA Protein Assay Kit (PC0020, Solarbio). Equal amount (20 μg) heat-denatured proteins were subjected into each lane and separated on SDS-PAGE gels by electrophoresis. Then proteins were transferred onto polyvinylidene fluoride (PVDF) membranes. After 5 % non-fat milk blocking for 30min, PVDF membrane were incubated with primary antibodies at 4 °C overnight on a shaker, then anti-Rabbit IgG (SA00001-2, Proteintech) or anti-Mouse IgG (SA00001-1, Proteintech) was incubated for 1h at ambient temperature. Bands were detected by chemiluminescent Horseradish Peroxidase substrate (WBKLS0500, Merck Millipore), and visualized using a ChemiDoc™ touch imaging system (Bio-Rad, Hercules, CA, USA). Quantitative analysis of each band was performed using ImageJ software (version 1.53q).

4.12. Intracellular calcium oscillations

Fluo-4 AM dye (20552, AAT Bioquest) was used to measure the intracellular calcium oscillation according to our previous publication [26]. In brief, BMMs were seeded in 35 mm dishes at a density of 2×10^5 cells/ml and subjected to osteoclast-induction medium either with or without Loc14 (5 μM) for 24h. Cells were then changed into complete medium containing 5 μM fluo-4 AM and 0.05 % Pluronic F127 (Sigma) and incubated for 50min at 37 °C avoid from light. After twice washes using PBS, cells were incubated in an isotonic solution (ISO) (Supplementary material 4) and then ready for fluorescent observation. Live cell imaging analysis involved continuous recording of fluorescence intensity for 20 min at 5-s intervals, using a fluorescence microscope (EVOS M7000, Invitrogen) with excitation wavelength at 488 nm and emission wavelength range from 505 to 530 nm. The fluorescence data was then quantified by Image J software (version 1.53q).

To monitor the intensity changes of intracellular Ca^{2+} fluorescence during extracellular Ca^{2+} influx or release from the ER in cells, Ca^{2+}-free isotonic solution (ISO) was employed after fluo-4 AM incubation. Once the cytosolic Ca^{2+} level returned to a stable baseline, 1 μM Thapsigargin (TG) (Sigma-Aldrich) was added to the Ca^{2+} free ISO to induce ER Ca^{2+} release, or Ca^{2+} free ISO supplemented with 2.6 mM $CaCl_2$ (a 2-fold Ca^{2+} concentration) was used to stimulate extracellular Ca^{2+} influx. Change of fluorescence intensity was recorded using the aforementioned methodology, and intensity of intracellular Ca^{2+} fluorescence was normalized to the initial Ca^{2+} level within the cell.

Table 1
Primer sequences for qPCR.

Target (GenBank accession no.)	Primers	Product length (bp)
Traf6 (NM_001303273.1)	F: AAAGCGAGAGATTCTTTCCCTG	125
	R: ACTGGGGACAATTCACTAGAGC	
Nfatc1 (NM_001164109.1)	F: CCGTTGCTTCCAGAAAATAACA	152
	R: TGTGGGATGTGAACTCGGAA	
Ctsk (NM_007802.4)	F: CTTCCAATACGTGCAGCAGA	155
	R: TCTTCAGGGCTTTCTCGTTC	
Trpc1 (NM_001311123.2)	F: GCAATGACACCTTCCACTCGTT	147
	R: AAGTTCCAACAATCACAGCTCCAA	
Trpc4 (NM_001253682.1)	F: GCGTGCTGCTGATAACTTGAG	133
	R: TTCCTTAACATTCTCCTCCGTCAA	
Itpr1 (XM_006505623.1)	F: CCACCAATGCTGACATCCTGATT	117
	R: GCCACACCTCTTCCTCATCCT	
Calr (NM_007591.3)	F: GAGCAGTTCTTGGACGGAGAT	150
	R: AAATCGGGCATCTTGGCTTGT	
Stim1 (NM_001374058.1)	F: TGGACTGTGGATGAGGTGATAC	127
	R: TGGTGGTGTTGGTTACTGCTA	
Orai1 (NM_175423.3)	F: TGCTCTGCTGGGTCAAGTTCT	94
	R: TGGTTGGCGACGATGACTGAT	
Canx (NM_001110499.1)	F: CCTTGTGATCCTCTTCTGCTGTT	149
	R: GCTTCTCCTCTTCTTCCTCTTCAT	
Calm1 (NM_001313934.1)	F: GGCACCATCACAACCAAGGAA	104
	R: CCATCAGCATCCACTTCGTTGA	
Calcineurin (NM_008913.5)	F: GCCAGAGTGTTCTCAGTTCTCAG	145
	R: CAGCCTCAATAGCCTCAACAGTAG	
GAPDH (XM_036165840.1)	F: ACTTTGTCAAGCTCATTTCC	267
	R: TGCAGCGAACTTTATTGATG	

4.13. Ovariectomy (OVX)-Induced osteoporosis model

Eight weeks old C57BL/6J female mice were randomly split into three groups (sham group, OVX group and OVX + Loc14 group) (n = 5 in each group). The latter two groups underwent bilateral ovariectomy under anesthesia as previously reported [63]. Briefly, dorsal incision was made and ovaries were then excised. The sham group only received peripheral ovarian lipectomy. After 1 week recuperation, mice in OVX + Loc14 group received intraperitoneal injection of Loc14 (5 mg/kg) every other day, while sham and OVX group received an equal volume of normal saline in the same approach. Four weeks after first dosage, all mice were euthanized for sample collection.

4.14. Micro-CT scanning

Soft tissue was carefully removed, and femurs were collected and fixed with 4 % PFA for 24h, then rinsed and soaked in 70 % ethanol. The distal femurs were scanned by MicroCT (vivaCT 80, SCANCO) with the following settings: 70 kVp, 114 μA, and 8 W. Approximately 10–210 (2 mm) above the highest point of the growth plate at the distal femur was chosen as the region of interest (ROI) for subsequent analysis. The following parameter, including bone volume fraction (BV/TV), trabecular number (Tb.N), trabecular separation (Tb.Sp), trabecular thickness (Tb.Th), and three-dimensional (3D) images were obtained using the CT Analyzer program [5].

4.15. Histology

This procedure was performed following our previous protocol [5,61]. After finishing CT scanning, fixed femurs were soaked in 20 % sucrose/PBS for 12h at 4 °C for dehydration, then embedded into optimal cutting temperature (OCT) for 6h at 4 °C, followed by frozen into new OCT over 12h at −80 °C. Undecalcified femurs were then cryosectioned at 7 μm using the cryostat microtome (Minux FS800, RWD Inc.) under the assistance of Cryofilm tape (Section Lab, Hiroshima, Japan). Crytosections were then immersed into PBS for 30min, and stained with TRAP solution for 15min at 37 °C. After that, the section counterstained with methyl green (C0115, Beyotime) for 10min, or Weigert hematoxylin solution (G1142, Solarbio) for 4min at RT. Images were pictured by a fluorescence microscope (nib620fl, Nexcope). TRAP positive cells were calculated by ImageJ software (version 1.53q).

4.16. Double calcein labeling assay

Mice were double-labeled with calcein (20 mg/kg, Sigma-Aldrich) through intraperitoneal injection at 12 and 3 days before euthanasia. Undecalcified femurs were cryosectioned at 7 μm using Cryofilm tape (Section Lab, Hiroshima, Japan). Images of calcein labeling were captured by a fluorescence microscope (nib620 fl, Nexcope), and parameters including inter-label width, bone mineral apposition rate (MAR) and bone formation rate (BFR) were measured.

4.17. Statistical analysis

Experiments in this study were repeated from three independent biological samples. All data were showed as mean ± standard deviation (SD). Student t-test was applied for two groups comparison, while one-way ANOVA was used for multiple comparison. GraphPad Prism 8.0 (version 6, GraphPad Software, San Diego, CA, United States) software was used for statistical analyses, and $p < 0.05$ was considered as statistically significant.

Ethics approval and consent to participate

All experiments involving mice were performed following the protocol approved by the Institutional Animal Care and Use Committee (IACUC) of the Shandong Provincial Hospital Affiliated to Shandong First Medical University (Shandong, China; No.2023-034).

Data availability statement

The datasets used and/or analyzed during the current study are available from the corresponding author on reasonable request.

CRediT authorship contribution statement

Tao Yuan: Writing – original draft, Methodology, Investigation, Formal analysis, Data curation, Conceptualization. **Yi Wang:** Writing – original draft, Validation, Formal analysis, Data curation, Conceptualization. **Haojue Wang:** Supervision, Software, Methodology, Formal analysis, Conceptualization. **Qizhen Lu:** Validation, Software, Formal analysis, Conceptualization. **Xin Zhang:**

Supervision, Software, Methodology, Conceptualization. **Ziqing Li:** Writing – review & editing, Supervision, Funding acquisition, Data curation, Conceptualization. **Shui Sun:** Writing – review & editing, Supervision, Funding acquisition, Conceptualization.

Declaration of competing interest

The authors declare that they have no competing interests.

Acknowledgments

Draft of Fig.9 was created with BioRender.com.

Appendix A. Supplementary data

Supplementary data to this article can be found online at https://doi.org/10.1016/j.heliyon.2024.e35374.

References

[1] J.S. Yu, N.G. Krishna, M.G. Fox, D.G. Blankenbaker, M.A. Frick, S.T. Jawetz, G. Li, C. Reitman, N. Said, J.D. Stensby, N. Subhas, M. Tulchinsky, E.A. Walker, F. D. Beaman, ACR appropriateness Criteria® osteoporosis and bone mineral density: 2022 update, J. Am. Coll. Radiol. 19 (11s) (2022) S417–s432.

[2] Management of postmenopausal osteoporosis: ACOG clinical practice guideline No. 2, Obstet. Gynecol. 139 (4) (2022) 698–717.

[3] L. Wang, W. Yu, X. Yin, L. Cui, S. Tang, N. Jiang, L. Cui, N. Zhao, Q. Lin, L. Chen, H. Lin, X. Jin, Z. Dong, Z. Ren, Z. Hou, Y. Zhang, J. Zhong, S. Cai, Y. Liu, R. Meng, Y. Deng, X. Ding, J. Ma, Z. Xie, L. Shen, W. Wu, M. Zhang, Q. Ying, Y. Zeng, J. Dong, S.R. Cummings, Z. Li, W. Xia, Prevalence of osteoporosis and fracture in China: the China osteoporosis prevalence study, JAMA Netw. Open 4 (8) (2021) e2121106.

[4] M.Y. Tu, K.Y. Han, G.R. Chang, G.D. Lai, K.Y. Chang, C.F. Chen, J.C. Lai, C.Y. Lai, H.L. Chen, C.M. Chen, Kefir peptides prevent estrogen deficiency-induced bone loss and modulate the structure of the gut microbiota in ovariectomized mice, Nutrients 12 (11) (2020).

[5] Y. Wang, T. Yuan, H. Wang, Q. Meng, H. Li, C. Feng, Z. Li, S. Sun, Inhibition of protein disulfide isomerase attenuates osteoclast differentiation and function via the readjustment of cellular redox state in postmenopausal osteoporosis, Inflammation 47 (2) (2023) 626–648.

[6] R. Wang, Y. Yang, Z. Zhang, N. Zhao, E.A.C. Wiemer, J. Ben, J. Ma, L. Yuan, Major vault protein (MVP) suppresses aging- and estrogen deficiency-related bone loss through Fas-mediated apoptosis in osteoclasts, Cell Death Dis. 14 (9) (2023) 604.

[7] L. Lin, Z. Guo, E. He, X. Long, D. Wang, Y. Zhang, W. Guo, Q. Wei, W. He, W. Wu, J. Li, L. Wo, D. Hong, J. Zheng, M. He, Q. Zhao, SIRT2 regulates extracellular vesicle-mediated liver-bone communication, Nat. Metab. 5 (5) (2023) 821–841.

[8] S.J. Lee, S.A. Jang, S.C. Kim, D.R. Gu, H. Yang, J.A. Ryuk, H. Ha, Euonymus alatus (thunb.) siebold prevents osteoclast differentiation and osteoporosis, Nutrients 15 (18) (2023).

[9] Q. Meng, Y. Wang, T. Yuan, Y. Su, Z. Li, S. Sun, Osteoclast: the novel whistleblower in osteonecrosis of the femoral head, Gene Reports 33 (2023) 101833.

[10] H. Okada, K. Okabe, S. Tanaka, Finely-tuned calcium oscillations in osteoclast differentiation and bone resorption, Int. J. Mol. Sci. 22 (1) (2020).

[11] H. Wang, T. Yuan, Y. Wang, C. Liu, D. Li, Z. Li, S. Sun, Osteoclasts and osteoarthritis: novel intervention targets and therapeutic potentials during aging, Aging Cell (2024) e14092.

[12] H. Chen, Y. Zhang, T. Yu, G. Song, T. Xu, T. Xin, Y. Lin, B. Han, Nano-based drug delivery systems for periodontal tissue regeneration, Pharmaceutics 14 (10) (2022).

[13] H.J. Kim, J. Lee, G.R. Lee, N. Kim, H.I. Lee, M. Kwon, N.Y. Kim, J.H. Park, Y.H. Kang, H.J. Song, T. Kim, D.M. Shin, W. Jeong, Flunarizine inhibits osteoclastogenesis by regulating calcium signaling and promotes osteogenesis, J. Cell. Physiol. 236 (12) (2021) 8239–8252.

[14] M. Xu, D. Song, X. Xie, Y. Qin, J. Huang, C. Wang, J. Chen, Y. Su, J. Xu, Z. Zhao, Q. Liu, CGK733 alleviates ovariectomy-induced bone loss through blocking RANKL-mediated Ca(2+) oscillations and NF-κB/MAPK signaling pathways, iScience 26 (10) (2023) 107760.

[15] H. Huynh, Y. Wan, mTORC1 impedes osteoclast differentiation via calcineurin and NFATc1, Commun. Biol. 1 (2018) 29.

[16] D.Z. Lu, W. Dong, X.J. Feng, H. Chen, J.J. Liu, H. Wang, L.Y. Zang, M.C. Qi, CaMKII(δ) regulates osteoclastogenesis through ERK, JNK, and p38 MAPKs and CREB signalling pathway, Mol. Cell. Endocrinol. 508 (2020) 110791.

[17] H. Okada, H. Kajiya, Y. Omata, T. Matsumoto, Y. Sato, T. Kobayashi, S. Nakamura, Y. Kaneko, S. Nakamura, T. Koyama, S. Sudo, M. Shin, F. Okamoto, H. Watanabe, N. Tachibana, J. Hirose, T. Saito, T. Takai, M. Matsumoto, M. Nakamura, K. Okabe, T. Miyamoto, S. Tanaka, CTLA4-Ig directly inhibits osteoclastogenesis by interfering with intracellular calcium oscillations in bone marrow macrophages, J. Bone Miner. Res. 34 (9) (2019) 1744–1752.

[18] X. Li, L. Wang, H. Wang, A. Qin, X. Qin, Ano5 modulates calcium signaling during bone homeostasis in gnathodiaphyseal dysplasia, NPJ Genom Med 7 (1) (2022) 48.

[19] G. Paglia, M. Minacori, G. Meschiari, S. Fiorini, S. Chichiarelli, M. Eufemi, F. Altieri, Protein disulfide isomerase A3 (PDIA3): a pharmacological target in glioblastoma? Int. J. Mol. Sci. 24 (17) (2023).

[20] S. Chichiarelli, F. Altieri, G. Paglia, E. Rubini, M. Minacori, M. Eufemi, ERp57/PDIA3: new insight, Cell. Mol. Biol. Lett. 27 (1) (2022) 12.

[21] C.A. Di Buduo, V. Abbonante, C. Marty, F. Moccia, E. Rumi, D. Pietra, P.M. Soprano, D. Lim, D. Cattaneo, A. Iurlo, U. Gianelli, G. Barosi, V. Rosti, I. Plo, M. Cazzola, A. Balduini, Defective interaction of mutant calreticulin and SOCE in megakaryocytes from patients with myeloproliferative neoplasms, Blood 135 (2) (2020) 133–144.

[22] R. Wei, J. Qiao, D. Cui, Q. Pan, L. Guo, Screening and identification of hub genes in the development of early diabetic kidney disease based on weighted gene Co-expression network analysis, Front. Endocrinol. 13 (2022) 883658.

[23] N. Chamberlain, M. Ruban, Z.F. Mark, S.R. Bruno, A. Kumar, R. Chandrasekaran, D. Souza De Lima, D. Antos, E.M. Nakada, J.F. Alcorn, V. Anathy, Protein disulfide isomerase A3 regulates influenza neuraminidase activity and influenza burden in the lung, Int. J. Mol. Sci. 23 (3) (2022).

[24] N. Chamberlain, B.R. Korwin-Mihavics, E.M. Nakada, S.R. Bruno, D.E. Heppner, D.G. Chapman, S.M. Hoffman, A. van der Vliet, B.T. Suratt, O. Dienz, J. F. Alcorn, V. Anathy, Lung epithelial protein disulfide isomerase A3 (PDIA3) plays an important role in influenza infection, inflammation, and airway mechanics, Redox Biol. 22 (2019) 101129.

[25] A. Kumar, E. Elko, S.R. Bruno, Z.F. Mark, N. Chamberlain, B.K. Mihavics, R. Chandrasekaran, J. Walzer, M. Ruban, C. Gold, Y.W. Lam, S. Ghandikota, A. G. Jegga, J.L. Gomez, Y.M. Janssen-Heininger, V. Anathy, Inhibition of PDIA3 in club cells attenuates osteopontin production and lung fibrosis, Thorax 77 (7) (2022) 669–678.

[26] Z. Li, T. Liu, A. Gilmore, N.M. Gómez, C. Fu, J. Lim, S. Yang, C.H. Mitchell, Y.P. Li, M.J. Oursler, S. Yang, Regulator of G Protein signaling protein 12 (Rgs12) controls mouse osteoblast differentiation via calcium channel/oscillation and gαi-ERK signaling, J. Bone Miner. Res. 34 (4) (2019) 752–764.

[27] H. Wang, J. Swore, S. Sharma, J.R. Szymanski, R. Yuste, T.L. Daniel, M. Regnier, M.M. Bosma, A.L. Fairhall, A complete biomechanical model of Hydra contractile behaviors, from neural drive to muscle to movement, Proc Natl Acad Sci U S A 120 (11) (2023) e2210439120.

[28] H. Okada, S. Tanaka, Plasmalemmal interface for calcium signaling in osteoclast differentiation, Curr. Opin. Cell Biol. 74 (2022) 55–61.

[29] D. Prins, J. Groenendyk, N. Touret, M. Michalak, Modulation of STIM1 and capacitative Ca2+ entry by the endoplasmic reticulum luminal oxidoreductase ERp57, EMBO Rep. 12 (11) (2011) 1182–1188.

[30] M. Doroudi, Z. Schwartz, B.D. Boyan, Membrane-mediated actions of 1,25-dihydroxy vitamin D3: a review of the roles of phospholipase A2 activating protein and Ca(2+)/calmodulin-dependent protein kinase II, J. Steroid Biochem. Mol. Biol. 147 (2015) 81–84.

[31] K. Inoue, X. Hu, B. Zhao, Regulatory network mediated by RBP-J/NFATc1-miR182 controls inflammatory bone resorption, Faseb. J. 34 (2) (2020) 2392–2407.

[32] S. Mak, W. Li, H. Fu, J. Luo, W. Cui, S. Hu, Y. Pang, P.R. Carlier, K.W. Tsim, R. Pi, Y. Han, Promising tacrine/huperzine A-based dimeric acetylcholinesterase inhibitors for neurodegenerative disorders: from relieving symptoms to modifying diseases through multitarget, J. Neurochem. 158 (6) (2021) 1381–1393.

[33] Q. He, K. Fu, H. Yao, S. Wei, L. Xiang, S. Liu, T. Chen, Y. Gao, Traditional Chinese decoction Si Zhi Wan attenuates ovariectomy (OVX)-induced bone loss by inhibiting osteoclastogenesis and promoting apoptosis of mature osteoclasts, Front. Pharmacol. 13 (2022) 983884.

[34] J. Kular, J. Tickner, S.M. Chim, J. Xu, An overview of the regulation of bone remodelling at the cellular level, Clin. Biochem. 45 (12) (2012) 863–873.

[35] I. Griswold-Prenner, A.K. Kashyap, S. Mazhar, Z.W. Hall, H. Fazelinia, H. Ischiropoulos, Unveiling the human nitroproteome: protein tyrosine nitration in cell signaling and cancer, J. Biol. Chem. 299 (8) (2023) 105038.

[36] H.Y. Shen, J.L. Xu, Z. Zhu, H.P. Xu, M.X. Liang, D. Xu, W.Q. Chen, J.H. Tang, Z. Fang, J. Zhang, Integration of bioinformatics and machine learning strategies identifies APM-related gene signatures to predict clinical outcomes and therapeutic responses for breast cancer patients, Neoplasia 45 (2023) 100942.

[37] L.M. Holbrook, P. Sasikumar, R.G. Stanley, A.D. Simmonds, A.B. Bicknell, J.M. Gibbins, The platelet-surface thiol isomerase enzyme ERp57 modulates platelet function, J Thromb Haemost 10 (2) (2012) 278–288.

[38] A. Hettinghouse, R. Liu, C.J. Liu, Multifunctional molecule ERp57: from cancer to neurodegenerative diseases, Pharmacol. Ther. 181 (2018) 34–48.

[39] Y. Wang, J. Chen, C.S. Lee, A. Nizkorodov, K. Riemenschneider, D. Martin, S. Hyzy, Z. Schwartz, B.D. Boyan, Disruption of Pdia3 gene results in bone abnormality and affects 1alpha,25-dihydroxy-vitamin D3-induced rapid activation of PKC, J. Steroid Biochem. Mol. Biol. 121 (1–2) (2010) 257–260.

[40] Y. Wang, A. Nizkorodov, K. Riemenschneider, C.S. Lee, R. Olivares-Navarrete, Z. Schwartz, B.D. Boyan, Impaired bone formation in Pdia3 deficient mice, PLoS One 9 (11) (2014) e112708.

[41] A. Linz, Y. Knieper, T. Gronau, U. Hansen, A. Aszodi, N. Garbi, G.J. Hämmerling, T. Pap, P. Bruckner, R. Dreier, ER stress during the pubertal growth spurt results in impaired long-bone growth in chondrocyte-specific ERp57 knockout mice, J. Bone Miner. Res. 30 (8) (2015) 1481–1493.

[42] M.K. Boag, L. Ma, G.D. Mellick, D.L. Pountney, Y. Feng, R.J. Quinn, A.W. Liew, M. Dharmasivam, M.G. Azad, R. Afroz, D.R. Richardson, Calcium channels and iron metabolism: a redox catastrophe in Parkinson's disease and an innovative path to novel therapies? Redox Biol. 47 (2021) 102136.

[43] J.Y. Kang, N. Kang, Y.M. Yang, J.H. Hong, D.M. Shin, The role of Ca(2+)-NFATc1 signaling and its modulation on osteoclastogenesis, Int. J. Mol. Sci. 21 (10) (2020).

[44] G. Kodakandla, S.J. West, Q. Wang, R. Tewari, M.X. Zhu, A.M. Akimzhanov, D. Boehning, Dynamic S-acylation of the ER-resident protein stromal interaction molecule 1 (STIM1) is required for store-operated Ca(2+) entry, J. Biol. Chem. 298 (9) (2022) 102303.

[45] F. Moccia, V. Brunetti, A. Perna, G. Guerra, T. Soda, R. Berra-Romani, The molecular heterogeneity of store-operated Ca(2+) entry in vascular endothelial cells: the different roles of Orai1 and TRPC1/TRPC4 channels in the transition from Ca(2+)-selective to non-selective cation currents, Int. J. Mol. Sci. 24 (4) (2023).

[46] J. Xie, G. Ma, L. Zhou, L. He, Z. Zhang, P. Tan, Z. Huang, S. Fang, T. Wang, Y.T. Lee, S. Wen, S. Siwko, L. Wang, J. Liu, Y. Du, N. Zhang, X. Liu, L. Han, Y. Huang, R. Wang, Y. Wang, Y. Zhou, W. Han, Identification of a STIM1 splicing variant that promotes glioblastoma growth, Adv. Sci. 9 (11) (2022) e2103940.

[47] D. Prins, C. González Arias, T. Klampfl, J. Grinfeld, A.R. Green, Mutant calreticulin in the myeloproliferative neoplasms, Hemasphere 4 (1) (2020) e333.

[48] M. Irnaten, C.J. O'Brien, Calcium-Signalling in human glaucoma lamina cribrosa myofibroblasts, Int. J. Mol. Sci. 24 (2) (2023).

[49] Y.J. Park, S.A. Yoo, M. Kim, W.U. Kim, The role of calcium-calcineurin-NFAT signaling pathway in health and autoimmune diseases, Front. Immunol. 11 (2020) 195.

[50] C. Barceló, P. Sisó, O. Maiques, I. de la Rosa, R.M. Martí, A. Macià, T-type calcium channels: a potential novel target in melanoma, Cancers 12 (2) (2020).

[51] Z. Sun, X. Cao, Z. Zhang, Z. Hu, L. Zhang, H. Wang, H. Zhou, D. Li, S. Zhang, M. Xie, Simulated microgravity inhibits L-type calcium channel currents partially by the up-regulation of miR-103 in MC3T3-E1 osteoblasts, Sci. Rep. 5 (2015) 8077.

[52] W. Lasoń, D. Jantas, M. Leśkiewicz, M. Regulska, A. Basta-Kaim, Vitamin D3 and ischemic stroke: a narrative review, Antioxidants 11 (11) (2022).

[53] M.A. Żmijewski, Nongenomic activities of vitamin D, Nutrients 14 (23) (2022).

[54] W.S. Yang, H. Yu, J.J. Kim, M.J. Lee, S.K. Park, Vitamin D-induced ectodomain shedding of TNF receptor 1 as a nongenomic action: D3 vs D2 derivatives, J. Steroid Biochem. Mol. Biol. 155 (Pt A) (2016) 18–25.

[55] H.Y. Lee, K.M. Cho, M.K. Kim, M. Lee, H. Kim, C.Y. Choi, K.K. Kim, J.S. Park, H.H. Kim, Y.S. Bae, Sphingosylphosphorylcholine blocks ovariectomy-induced bone loss by suppressing Ca(2+)/calmodulin-mediated osteoclast differentiation, J. Cell Mol. Med. 25 (1) (2021) 473–483.

[56] J. Chen, R. Olivares-Navarrete, Y. Wang, T.R. Herman, B.D. Boyan, Z. Schwartz, Protein-disulfide isomerase-associated 3 (Pdia3) mediates the membrane response to 1,25-dihydroxyvitamin D3 in osteoblasts, J. Biol. Chem. 285 (47) (2010) 37041–37050.

[57] Y. Wu, D.W. Essex, Vascular thiol isomerases in thrombosis: the yin and yang, J Thromb Haemost 18 (11) (2020) 2790–2800.

[58] W. Hu, L. Zhang, M.X. Li, J. Shen, X.D. Liu, J.W. Li, I.H.T. Ho, J.C.Y. Wu, C.K.Y. Cheung, Y.C. Zhang, A.H.Y. Lau, H. Ashktorab, D.T. Smoot, E. F. Fang, M.T.V. Chan, T. Gin, W. Gong, W.K.K. Wu, C.H. Cho, Vitamin D3 activates the autolysosomal degradation function against Helicobacter pylori through the PDIA3 receptor in gastric epithelial cells, Autophagy 15 (4) (2019) 707–725.

[59] C. Wang, Y. Zhu, D. Wu, Z. Wang, X. Xu, Y. Shi, G. Yang, Y. Yu, X. Peng, The role of PDIA3 in myogenesis during muscle regeneration, Exp. Mol. Med. 52 (1) (2020) 105–117.

[60] Z.Q. Li, C.H. Li, CRISPR/Cas9 from bench to bedside: what clinicians need to know before application? Mil Med Res 7 (1) (2020) 61.

[61] A.Y.H. Ng, Z. Li, M.M. Jones, S. Yang, C. Li, C. Fu, C. Tu, M.J. Oursler, J. Qu, S. Yang, Regulator of G protein signaling 12 enhances osteoclastogenesis by suppressing Nrf2-dependent antioxidant proteins to promote the generation of reactive oxygen species, Elife 8 (2019).

[62] Z. Cui, C. Feng, J. Chen, Y. Wang, Q. Meng, S. Zhao, Y. Zhang, D. Feng, Z. Li, S. Sun, Network pharmacology deciphers the action of bioactive polypeptide in attenuating inflammatory osteolysis via the suppression of oxidative stress and restoration of bone remodeling balance, Oxid. Med. Cell. Longev. 2022 (2022) 4913534.

[63] D. Li, J. Liu, B. Guo, C. Liang, L. Dang, C. Lu, X. He, H.Y. Cheung, L. Xu, C. Lu, B. He, B. Liu, A.B. Shaikh, F. Li, L. Wang, Z. Yang, D.W. Au, S. Peng, Z. Zhang, B. T. Zhang, X. Pan, A. Qian, P. Shang, L. Xiao, B. Jiang, C.K. Wong, J. Xu, Z. Bian, Z. Liang, D.A. Guo, H. Zhu, W. Tan, A. Lu, G. Zhang, Osteoclast-derived exosomal miR-214-3p inhibits osteoblastic bone formation, Nat. Commun. 7 (2016) 10872.